1980

Electronic structure of zirconium sulfide

Thuy-Hoa Nguyen
Iowa State University

NGUYEN, THUY-HOA

ELECTRONIC STRUCTURE OF ZIRCONIUM-SULFIDE

Iowa State University PH.D. 1980

Electronic structure of zirconium sulfide

by

Thuy-Hoa Nguyen

A Dissertation Submitted to the
Graduate Faculty in Partial Fulfillment of the
Requirements for the Degree of
DOCTOR OF PHILOSOPHY

Department: Chemistry
Major: Physical Chemistry

Approved:

Signature was redacted for privacy.

Signature was redacted for privacy.

In Charge of Major Work

Signature was redacted for privacy.

For the Major Department

Signature was redacted for privacy.

For the Graduate College

Iowa State University
Ames, Iowa

1980

TABLE OF CONTENTS

		Page
I.	INTRODUCTION	1
II.	ZrS_{1-x} AND ZrS_{1+x} SAMPLES	4
	A. Previous Work	4
	B. Sample Preparation	5
	C. Sample Analysis	6
	D. Results and Discussion	7
III.	ELECTRONIC STRUCTURE CALCULATIONS	10
	A. Background	10
	B. Results and Discussion	18
IV.	PHOTOELECTRON SPECTROSCOPY	56
	A. Introduction	56
	B. Experiment	56
	C. Results and Discussion	58
V.	ELECTRONIC HEAT CAPACITY	63
	A. Background	63
	B. Experiment	65
	C. Results and Discussion	70
VI.	SUMMARY AND CONCLUSION	77
VII.	REFERENCES	80
VIII.	ACKNOWLEDGEMENTS	84

I. INTRODUCTION

The research described below was carried out to provide a quantitative theoretical basis for the discussion of bonding in the case of two elementary structures (NaCl-type and WC-type), both of which occur in the Zr-S system.

The NaCl and WC structures are often described in terms of stacking sequences of hexagonal layers of atoms. With the stacking positions A, B, C of hexagonal layers of atoms, as shown in Fig. 1.1a, the alternate layers of metal atoms and nonmetal atoms are stacked in the ABCABC... sequence for the NaCl structure, and in the ABAB... sequence for the WC structure. The NaCl structure and WC structure and their projections on a hexagonal (110) plane are shown in Figs. 1.1b-1.1e. In the case of the NaCl structure type, the metal atom layers are between two nonmetal atom layers, which project along the (111) direction onto different hexagonal planes and vice versa; a metal atom layer that projects onto positions A is sandwiched between two nonmetal atom layers projected onto positions B and C. As a result of this stacking sequence, both metal and nonmetal atoms have trigonal antiprismatic or octahedral coordination.

On the other hand, in the WC structure both metal and nonmetal atoms exhibit trigonal prismatic coordination.

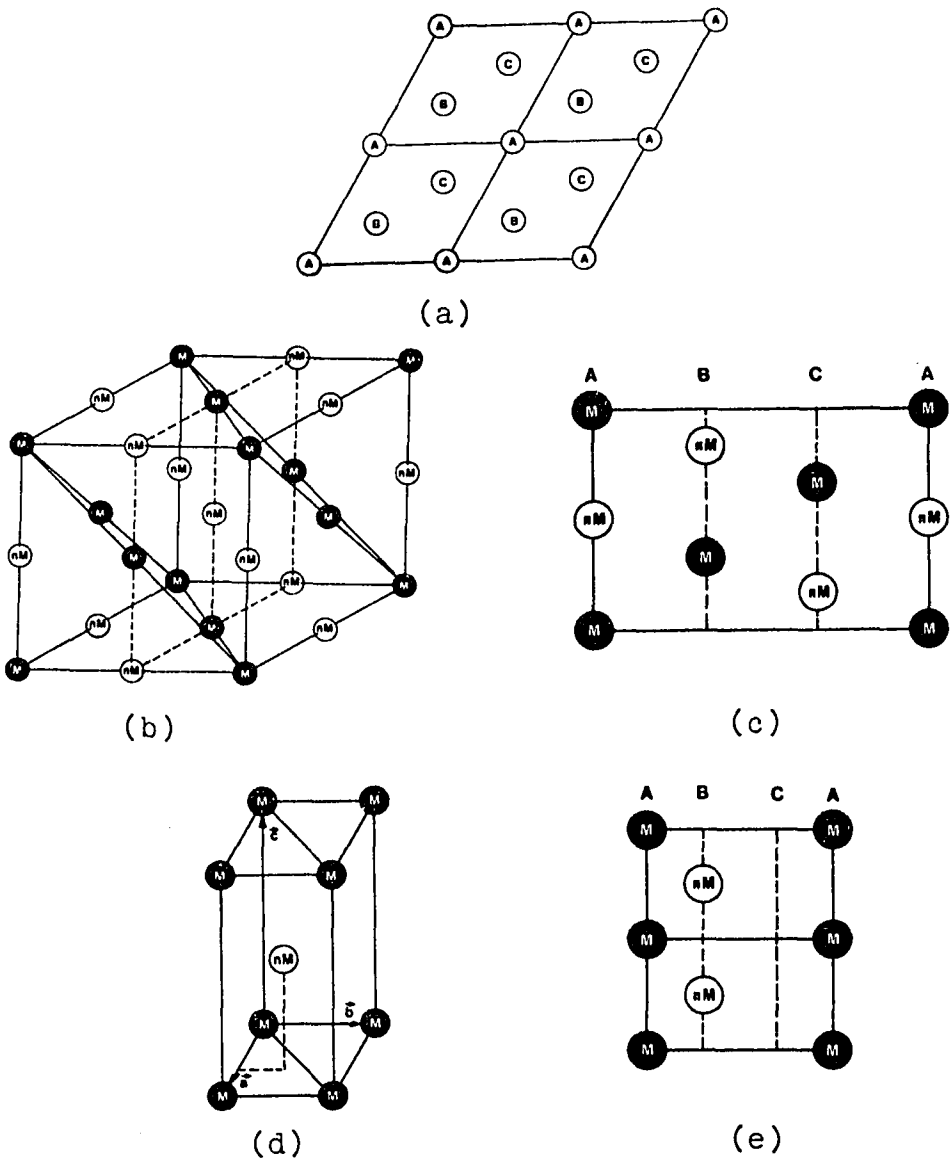

Fig. 1.1. Unit cell and stacking sequences for the NaCl-type and WC-type structures. (a) Projection of B and C sites on hexagonal plane containing A sites; (b) NaCl-type structure, the triangles indicate an octahedral coordination of nonmetal atom; (c) NaCl drawn on the hexagonal (110) plane; (d) WC-type structure; (e) WC drawn on the hexagonal (110) plane

As listed in table 1 of Ref. (1a), many transition metal compounds exist with the NaCl structure, or with the WC structure, or with the structures such as the NiAs structure (stacking sequence is ABACABAC...), the TiP structure (stacking sequence is ABACBABC...), etc., in which the coordination of the elements is similar to the coordination either in the NaCl structure (trigonal antiprismatic coordination) or in the WC structure (trigonal prismatic coordination). Therefore, the understanding of bonding in ZrS with the NaCl and WC structures will be useful in interpreting the bonding in many other compounds.

On the other hand, the WC structure by itself provides motivation for the electronic structure calculation of ZrS with the WC structure. It has been noted that WC, but not W, exhibits a catalytic activity similar to that of Pt (1b). It was suggested that this activity is related to the change in density of states at the Fermi energy upon going from elemental W to WC. Therefore, the electronic structure of ZrS with the WC structure could provide some insight into the catalytic behavior of the compound WC.

Explanation of dissertation format

The following text will be divided into 5 chapters. The second chapter will discuss the sample preparation of Zr-S samples. The third chapter will present the electronic

structure calculations for ZrS of NaCl and WC structure types. The fourth and fifth chapters will cover ESCA and electronic heat capacity studies which provide support for the calculations discussed in Chapter III. Finally, the summary and conclusion will be in the sixth chapter.

II. ZrS_{1-x} AND ZrS_{1+x} SAMPLES

A. Previous Work

The ZrS_{1-x} and ZrS_{1+x} phases of the Zr-S system have been studied by a number of investigators since 1939. Strotzer and coworkers were the first pioneers to investigate this system and reported $ZrS_{1.20} - ZrS_{1.49}$ compounds have a NaCl defect structure (2). Later on, Hahn et al. proposed $ZrS_{.9} - ZrS_{1.5}$ to be a NaCl superstructure, and reported that $ZrS_{.5} - ZrS_{.8}$ were formed with a WC structure type (3). McTaggert and Wadsley found that a defect NaCl structure of $ZrS_{.9} - ZrS_{1.6}$ has a primitive cubic unit cell, a = 10.25 Å (4). Conard and Franzen reported $ZrS_{.6} - ZrS_{.8}$ to be a WC structure type and $ZrS_{1.29}$, which is one of the ZrS_{1+x} compounds, occurred with a monoclinic cell, as a superstructure of NaCl type (5,6). More recently, Moodenbaugh (7) studied the superconductivity of the ZrS_{1+x} samples, which were found to exist with NaCl structure type with no superstructure cell.

According to Moodenbaugh, the ZrS_{1+x} compounds, NaCl structure type, are unstable with respect to decomposition into the ZrS_{1-x} with the WC structure type and the ZrS_{1+x} superstructure of the NaCl type, under an annealed treatment. Further, Moodenbaugh estimated the approximate composition of ZrS_{1-x} WC structure type to be $ZrS_{.9\pm.1}$.

B. Sample Preparation

The Zr-S samples were prepared directly from high purity grades of Zr and S elements. The zirconium was obtained from the Ames Laboratory with 99.9% purity. The sulfur used was 99.999% pure (obtained from Ventron Alfa products). The zirconium was rolled into the thin sheets (as thin as possible) about .003" thick. The sheets were cleaned either by chemical solution or electropolishing before use. For the phase and heat capacity studies, the zirconium sheets were cleaned in a chemical solution containing 10 volume percent hydrofluoric acid, 45 volume percent of nitric acid and the rest of water. The sheets were rinsed thoroughly in distilled water, ethanol and acetone in that order afterwards. For the photoelectron spectroscopy studies, the sheets were electropolished in 6% perchloric acid in a methanol bath maintained at -70°C with a current density about 0.2 A cm^{-2}. The electropolished sheets were rinsed with ethanol followed by acetone.

The sheets were cut into small pieces to be able to put through the sample tubes. The desired amounts of zirconium and sulfur (for the samples with starting composition in a range $.5 < S/Zr < 1.5$) were inserted in Vycor tubes which were previously outgassed using an oxygen-gas torch.

The sample tubes were evacuated to about 10^{-6} torr residual pressure, sealed and placed in a furnace. The gradient temperature in a furnace was set up to maintain the temperature difference between two ends of the sample tubes, one end for the zirconium metal at 650°C, and the other end for the sulfur condensed at 440°C - 500°C. It required about 2 days to one week (depending on initial composition of the samples) for all the sulfur to react with the zirconium. When the sulfur was no longer visible in the tubes, the solid reaction products were the sulfur rich compounds ZrS_2, ZrS_3 coating outside the unreacted zirconium metal sheets. To achieve the equilibrium more rapidly, the samples were transferred to tungsten crucibles. The samples in tungsten containers were then annealed at higher temperatures in a vacuum line of 10^{-6} torr residual pressure by the use of inductive heating. A schematic diagram of the vacuum line used for the high temperature annealing treatment is shown in Ref. (8). The samples were typically annealed for about 8-10 hrs at T = 1650°C - 1750°C for ZrS_{1-x} samples and at T = 1400°C - 1500°C for ZrS_{1+x} samples.

C. Sample Analysis

The phase and composition of the samples were analyzed.

1. Phase analysis

The phase of the samples was determined by a powder diffraction technique. The powder patterns were taken using a Model XDC-700 Guinier Camera (IRDAB, Stockholm) provided with a quartz, bent crystal monochromator adjusted to produce a CuK_α radiation (λ = 1.54056 Å). Si powder (NBS Standard Reference Material 640, a = 5.43088 Å) was mixed with samples and used as a standard. The powder patterns were checked against the computed powder patterns produced by the Yvon, Jeitschko and Parthé program (9). The limit of detection of powder diffraction was claimed to be about 3 atomic unit percent.

2. Combustion analysis

During the annealing step, some sulfur was driven off from the samples, some zirconium diffused inside the tungsten and some samples got stuck to the container. All of these changes caused the composition of the annealed samples to be unpredictable on the basis of starting composition and material balance. Therefore, the final compositions of the samples were analyzed by oxidizing them to ZrO_2 in Pt crucibles in air at 900°C.

D. Results and Discussion

The samples with a variety of compositions were prepared and analyzed to determine the homogeneity ranges of

the ZrS_{1-x} and ZrS_{1+x} phases. The following Table 2.1 will summarize the phases of some typical compounds. As listed

Table 2.1. The phases versus compositions

Composition (Combustion Results)	Phases
$ZrS_{.88}$	Zr_2S,[a] ZrS_{1-x}[b]
$ZrS_{.9}$	ZrS_{1-x}
$ZrS_{.99}$	ZrS_{1-x}
$ZrS_{1.05}$	ZrS_{1-x}, ZrS_{1+x}[c]
$ZrS_{1.21}$	ZrS_{1-x}, ZrS_{1+x}
$ZrS_{1.28}$	ZrS_{1+x}
$ZrS_{1.30}$	ZrS_{1+x}
$ZrS_{1.40}$	ZrS_{1+x}, unable to index one fuzzy line at a low angle

[a] Zr_2S has orthorhombic unit cell (10).

[b] ZrS_{1-x} is a WC structure type (5).

[c] ZrS_{1+x} has a monoclinic unit cell and is a NaCl superstructure (6).

in Table 2.1, from the observations of the phases of $ZrS_{.88}$ and $ZrS_{.9}$, the lower end of the homogeneity range of ZrS_{1-x} phase was concluded to be between $ZrS_{.88}$ and $ZrS_{.9}$. Similarly, the upper end of the homogeneity range was in a range $ZrS_{.99}$ and $ZrS_{1.05}$.

HfS compound at 1:1 composition is known to be a WC structure type (11). Both Hf and Zr elements are in group IV.B, and have the same Slater's radii (r = 1.55 Å) (12). Intuitively, ZrS most likely has the same structure as HfS does, at the 1:1 composition. In that case, the upper end of ZrS_{1-x} phase might include the compound ZrS.

With the data for ZrS_{1+x} compounds, the lower boundary of the homogeneous range ZrS_{1+x} was between $ZrS_{1.21}$ and $ZrS_{1.28}$; and the upper end limit was in a range of $ZrS_{1.30}$ - $ZrS_{1.40}$.

By using the described method for sample preparation, ZrS at a ratio 1:1 (3,6) with the NaCl structure and ZrS_{1+x} in the composition range ($ZrS_{1.05\pm.03}$ - $ZrS_{1.39}$) (7) could not be formed or detected within the limitations of sample analysis.

As a matter of fact, the results of this study show that the ZrS_{1+x} samples in the homogeneity range ($ZrS_{1.25\pm.04}$ - $ZrS_{1.35\pm.05}$) were formed with a monoclinic superstructure of NaCl-type, while samples with compositions in a range from $ZrS_{1.02\pm.03}$ to $ZrS_{1.25\pm.04}$ were identified

to be the mixtures of two phases ZrS_{1+x} (superstructure of NaCl-type) and ZrS_{1-x} (WC structure).

However, Moodenbaugh observed that $ZrS_{1.20}$ with the NaCl structure (no superstructure), prepared by the arc-melting method, was transformed to a mixture of two phases (ZrS_{1+x} with the superstructure of NaCl-type and ZrS_{1-x} with the WC structure), after annealing at 800°C. This observation suggests that the NaCl structure is a metastable phase for $ZrS_{1.20}$ at lower temperatures and is obtained as a consequence of the sample quenching by the arc-melting method, and also explains the fact that the ideal NaCl structure was not obtained in the present work.

III. ELECTRONIC STRUCTURE CALCULATIONS

A. Background

1. Energy bands

The electronic structure of the compounds ZrS of NaCl-type and WC-type were calculated, using the Linearized Augmented Plane Wave method (LAPW) (13). The LAPW method was originated from the Augmented Plane Wave method (APW), which was developed by Slater in 1937 (14), and has been reviewed in detail by Loucks (15). The basis for the LAPW calculation is the muffin tin potential approximation for the crystal. In this approximation, the potential is assumed spherically symmetric inside the muffin tin spheres, which are nonoverlapping spheres, centered at the atomic sites and filling the unit cell to a maximum extent. Outside the spheres, the potential is assumed constant.

The crystal charge density is taken to be a superposition of atomic charge densities calculated by the self-consistent Hartree-Fock-Slater method using the Herman and Skillman program (16). The procedure for evaluating the potential was developed by Matheiss (17).

The crystal potential was separated into two contributions, the coulombic component and the exchange component. The coulombic potential contribution was a result of the combination of the atomic coulombic potential and the

spherical terms of a Löwdin Alpha expansion (18) of the neighboring coulombic potentials.

The exchange potential contribution was calculated using the Slater's free electron exchange approximation (19).

$$V_{ex}(r) = - 6 \left(\frac{3}{8\pi} \rho(r)\right)^{1/3}, \tag{3.1}$$

where $\rho(r)$ is the crystal charge density, i.e., the sum of the atomic charge density and the spherical terms of the Löwdin Alpha expansion of the neighboring charge densities. As a consequence of the muffin potential, the basis functions have the following forms:

Outside the spheres:

$$\phi_{\vec{k}_i}(\vec{r}) = \frac{1}{\sqrt{\Omega}} \exp(i\vec{k}_i \cdot \vec{r}) \tag{3.2}$$

And inside the ν'th sphere:

$$\phi_{\vec{k}_i}(\vec{r}) = \exp(i\vec{k}_i \cdot \vec{r}_\nu) \sum_{\ell=0}^{N} \sum_{m=-\ell}^{m=+\ell} [A^{\nu}_{\ell,m} U_{\ell,E'}(\rho) + B^{\nu}_{\ell,m} \dot{U}_{\ell,E'}(\rho)] Y_{\ell,m}(\hat{\rho}) \tag{3.3}$$

where $\vec{k}_i = \vec{k} + \vec{K}_i$

$\vec{k}$: reduced wave vector,

$\vec{K}_i$: reciprocal lattice vector,

$|\vec{\rho}| = |\vec{r} - \vec{r}_\nu|, \qquad |\vec{\rho}| < R_\nu$,

R_ν = radius of the ν'th sphere,

$\vec{r}_\nu$ = the vector from the origin to the center of the ν'th sphere.

Ω = volume of the unit cell,

$U_{\ell,E'}(\rho)$ = radial solution of the Schrödinger equation, evaluated at energy E',

$$\dot{U}_{\ell,E'}(\rho) = \frac{d[U_{\ell,E'}(\rho)]}{dE} ,$$

N = infinity (idealistically)

= 12 (practically),

$A^{\nu}_{\ell,m}$ and $B^{\nu}_{\ell,m}$ = the coefficients determined by the continuity of the basis functions and their first derivatives at the sphere boundary,

$$A^{\nu}_{\ell,m} = \frac{4\pi}{\Omega^{\frac{1}{2}}} R_{\nu}^2 \exp(i\vec{k}_i \cdot \vec{r}_{\nu}) Y^*_{\ell,m}(\hat{k}_i)\, i^{\ell}\, a^{\nu}_{\ell}, \tag{3.4}$$

$$a^{\nu}_{\ell} = j'_{\ell}(\vec{k}_i \cdot \vec{R}_{\nu}) \dot{U}_{\ell,E'}(\rho) - j_{\ell}(\vec{k}_i \cdot \vec{R}_{\nu}) \dot{U}'_{\ell,E'}(\rho) \tag{3.5}$$

$$B^{\nu}_{\ell,m} = \frac{4\pi}{\Omega^{\frac{1}{2}}} R_{\nu}^2 \exp(i\vec{k}_i \cdot \vec{r}_{\nu}) Y^*_{\ell,m}(\hat{k}_i) i^{\ell} b^{\nu}_{\ell} , \tag{3.6}$$

$$b^{\nu}_{\ell} = j_{\ell}(\vec{k}_i \cdot \vec{R}_{\nu})\, U'_{\ell,E'}(\rho) - j'_{\ell}(\vec{k}_i \cdot \vec{R}_{\nu})\, U_{\ell,E'}(\rho) \tag{3.7}$$

$$U'_{\ell,E'}(\rho) = \frac{d}{d\rho} [U_{\ell,E'}(\rho)], \quad \text{and}$$

$$\dot{U}'_{\ell,E'}(\rho) = \frac{d}{d\rho} [\dot{U}_{\ell,E'}(\rho)] .$$

The crystal wave function was expanded as:

$$\psi_{\vec{k}}(\vec{r}) = \sum_{i=1}^{N_v} C_i(\vec{k}_i)\, \phi_{\vec{k}_i}(\vec{r}) , \tag{3.8}$$

where

C_i = coefficients determined variationally,

and

N_v = number of basis functions, determined from a convergence test of the eigenvalues at various k points (Ref. 20).

The wavefunctions and eigenvalues are determined, using the Raleigh-Ritz variational method (21), in which the energy

$$E_{\vec{k}} = \frac{\langle \psi_{\vec{k}} | H | \psi_{\vec{k}} \rangle}{\langle \psi_{\vec{k}} | \psi_{\vec{k}} \rangle} = \frac{\Sigma_{i,j} C_i^*(\vec{k}_i) C_j(\vec{k}_j) H_{ij}}{\Sigma_{i,j} C_i^*(\vec{k}_i) C_j(\vec{k}_j) S_{ij}} \tag{3.9}$$

was minimized with respect to the coefficients C_i. This leads to the standard eigenvalue problem:

$$\sum_j C_j(\vec{k}_j)(H_{ij} - E_{\vec{k}} S_{ij}) = 0, \tag{3.10}$$

or in a matrix notation

$$\underset{\sim}{H}\, \vec{C}(\vec{k}) = E_{\vec{k}}\, \underset{\sim}{S}\, \vec{C}(\vec{k}) \tag{3.11}$$

The matrix elements H_{ij} and S_{ij} have the following expressions.

$$S_{ij} = \delta_{ij} - \sum_\nu \left(\frac{4\pi R_\nu^2}{\Omega} \exp(i\vec{k}_{ji}\cdot\vec{r}_\nu)\right)\left[\frac{j_1(\vec{k}_{ji}\cdot\vec{R}_\nu)}{\bar{k}_{ji}} - R_\nu^2 \sum_\ell (2\ell+1) P_\ell(\hat{k}_i\cdot\hat{k}_j)\cdot s_{ij}^{\ell,\nu}\right] \tag{3.12}$$

$$H_{ij} = k_j^2 - \sum_{\nu} \left(\frac{4\pi R_\nu^2 \cdot \exp(i\vec{k}_{ji}\cdot\vec{R}_\nu)}{\Omega}\right)\left[k_j^2 \frac{j_1(\vec{k}_{ji}\cdot\vec{R}_\nu)}{\vec{k}_{ji}} - R_\nu^2 \sum_{\ell} (2\ell+1)P_\ell(\hat{k}_i\cdot\hat{k}_j)(E\, s_{ij}^{\ell,\nu} + a_\ell^\nu(\vec{k}_i)b_\ell^\nu(\vec{k}_j)\right] \quad (3.13)$$

where

$$s_{ij}^{\ell,\nu} = a_\ell^\nu(\vec{k}_i)a_\ell^\nu(\vec{k}_j) + b_\ell^\nu(\vec{k}_i)b_\ell^\nu(\vec{k}_j)N_\ell^\nu, \quad (3.14)$$

$$N_\ell^\nu = \int_o^{R_\nu} r^2\, \dot{U}_{\ell,E'}(r)\, \dot{U}_{\ell,E'}(r)\, dr, \quad (3.15)$$

and

$$\vec{k}_{ji} = \vec{k}_j - \vec{k}_i.$$

The coefficients of the wavefunctions and the eigenvalues in equation (3.11) were obtained by using the subroutines in the Eispack package of computer subroutines (22). The principles of the subroutines are discussed by Wilkinson (23) and Wilkinson and Reinsh (24).

2. Density of states

The density of states of an electronic system

$$N(E) = \frac{2\Omega}{(2\pi)^3} \sum_n \int d^3k\, \delta[E_n(\vec{k}) - E] \quad (3.16)$$

transforms to an integral over surfaces of constant energy

$$N(E) = \frac{2\Omega}{(2\pi)^3} \sum_n \int_{E_{\vec{k},n}=E} \frac{dS}{|\nabla_{\vec{k}} E|} \tag{3.17}$$

where

n = band index.

Using the Gilat-Raubenheimer method (25), Jepsen divided the Brillouin Zone into microtetrahedra. The tetrahedra are sufficiently small that linearity in energy can be assumed (26). The integral in equation (3.17) is substituted by the summation over the tetrahedra:

$$N(E) \cong \frac{2\Omega}{(2\pi)^3} \sum_n \sum_i \frac{S_n(E,\vec{k}_i)}{|\nabla_{\vec{k}} E|} \tag{3.18}$$

$$\equiv \sum_{n,i} N_{n,i}(E), \tag{3.19}$$

where

$S_n(E,\vec{k}_i)$ = the area of the energy plane within the ith tetrahedron of constant energy E.

For each energy band, the energy eigenvalues at the corners of the tetrahedron ε_1, ε_2, ε_3 and ε_4 are in order:

$$\varepsilon_1 \leq \varepsilon_2 \leq \varepsilon_3 \leq \varepsilon_4.$$

The eigenvalues ε_1, ε_2, ε_3 and ε_4 are evaluated from the energy fit functions:

$$E_{fit}(\vec{k}) = \sum_n C_n S_n(\vec{k}), \tag{3.20}$$

$$S_n(\vec{k}) = \frac{1}{g} \sum_{\alpha=1}^{g} \exp(i \cdot \{\alpha \vec{R}_n\} \cdot \vec{k}), \tag{3.21}$$

where

g = group order,

α = symmetry operation,

$\vec{R}_n$ = lattice vector, and

C_n = Fourier coefficients determined from least squares treatment of fitting the energy eigenvalues previously calculated at known k points.

The formulas for calculating $N_{n,i}$ (in equation 3.19) are derived by Jepsen and Andersen, as listed in Table 3.1.

Table 3.1. Formulas for evaluating $N_{n,i}$

	$N(\varepsilon_1,\varepsilon_2,\varepsilon_3,\varepsilon_4, V,E)$
$E \leq \varepsilon_1$	0
$\varepsilon_1 \leq E \leq \varepsilon_2$	$V_3 \cdot \frac{(E-\varepsilon_1)^2}{(\varepsilon_1-\varepsilon_2)\cdot\Delta 1}$
$\varepsilon_2 \leq E \leq \varepsilon_3$	$V_3 \cdot \frac{\Delta 1\cdot\Delta 2 - (E-M)^2}{\Delta 1\cdot\Delta 2}$
$\varepsilon_3 \leq E \leq \varepsilon_4$	$V_3 \cdot \frac{(E-\varepsilon_4)^2}{(\varepsilon_4-\varepsilon_3)\cdot\Delta 4}$
$\varepsilon_4 \leq E$	0

$$\Delta = \varepsilon_4 + \varepsilon_3 - \varepsilon_2 - \varepsilon_1$$

$$M = (\varepsilon_4 * \varepsilon_3 - \varepsilon_2 * \varepsilon_1)/\Delta$$

$$\Delta_i = \varepsilon_i - M$$

$$V1 = V/\Delta$$

$$V3 = 3 * V1$$

V = volume of the tetrahedron

3. The partial density of states

The density of states are decomposed into its angular momentum ℓ contributions, which are called the ℓ-partial density of states, $N_\ell(E)$. The ℓ-partial density of states is evaluated in the following form:

$$N_\ell(E) = \sum_{n,i} N_{n,i}(E) * P_{n,i,\ell} \qquad (3.22)$$

where

$P_{n,i,\ell}$ = Percentage ℓ-character of the crystal wavefunction inside muffin tin spheres, extended to the Wigner Seitz sphere limit in the n'th band and in the ith tetrahedron.

The radius of the ν'th Wigner Seitz sphere is evaluated with an expression:

$$r_{WS}^{\nu} = \frac{\text{Vol. of the unit cell}}{\sum_{\nu} V_{MT}^{\nu}} * r_{MT}^{\nu} \qquad (3.23)$$

where

r_{WS}^{ν} = Radius of the ν'th Wigner Seitz sphere,

r_{MT}^{ν} = Radius of the ν'th muffin tin sphere, and

V_{MT}^{ν} = Volume of the ν'th muffin tin sphere.

B. Results and Discussion

1. Detailed information of calculations

The nonrelativistic, nonself-consistent band structures of ZrS with the NaCl structure type and ZrS with the WC structure type were computed using the LAPW method. The parameters used in the calculations are listed in Table 3.2.

Table 3.2. Input parameters for the LAPW calculations

	ZrS (NaCl-type)	ZrS (WC-type)
Lattice constants	a = 5.160 Å[a]	a = 3.430 Å[b] c = 3.454 Å
Zr MT sphere radii	1.395 Å	1.439 Å
S MT sphere radii	1.156 Å	1.156 Å
Percentage coverage of unit cell by MT spheres	52	54
Zr WS sphere radii	1.735 Å	1.768 Å
S WS sphere radii	1.438 Å	1.421 Å
Zr-Zr distance	3.648 Å	3.430 Å(6) 3.454 Å(2)
Zr-S distance	2.580 Å	2.627 Å

[a]Ref. 8.

[b]Present work.

Using the muffin tin potential approximation, the crystal potential was approximated to be spherically symmetric inside the muffin tin spheres and to be constant outside the spheres. The potentials were evaluated by superimposing the charge densities of neutral Zr atoms ($4d^2 5s^2$) and the charge densities of neutral S atoms ($3s^2 3p^4$). It should be noted that Walch and Ellis (27) found that energy bands are not sensitive to the electronic configuration of component elements used in evaluating the potential. Thus, the potential at each atomic site included its own spherical atomic potential and the spherical terms of a Löwdin Alpha expansion of its neighboring atomic potentials within a specified distance. For example, 256 neighboring atoms in ZrS NaCl-type and 276 neighboring atoms in ZrS WC-type were included in evaluating the potentials.

The muffin tin spheres were chosen to minimize the constant potential regions without overlapping spheres. The radii were also chosen to have a ratio of the Zr and S muffin tin sphere radii to be close to a factor of 7/6. This ratio follows an empirical rule developed by Switendick for estimating the number of basis functions required to approximately equalize the convergence of both nonmetal valence states and transition metal valence states in the APW method (28). The radii of the muffin tin spheres in the two structures were chosen to be close to each other for a

better comparison, although, the radii of the Zr muffin tin spheres were slightly larger in WC-type than in NaCl-type. However, the results of the band structure calculations are not very sensitive to the choice of the atomic sphere radii, as demonstrated by Schwarz et al. (29).

2. ZrS NaCl-type

At centers of 89 cubical volume elements, which were distributed evenly within one forty-eighth of the first Brillouin zone, were chosen k points. At each selected k point, at least 9 eigenvalues and the corresponding eigenfunctions were evaluated. The list of 89 k points is found in Ref. 30.

In evaluating the eigenvalues and eigenfunctions, the energy E_ℓ' in equation (3.3) was used as the energy parameter to solve the Schrödinger's equation. For the positive eigenvalues, the energy parameters were defined differently at Zr atomic sites and at S atomic sites:

$$E_\ell'(Zr) = .50 \text{ Ry.} \quad \text{for } \ell = 0, 1, \ldots, 12, \text{ and}$$

$$E_\ell'(S) = .30 \text{ Ry.} \quad \text{for } \ell = 0, 1, \ldots, 12.$$

For the negative eigenvalues, the energy parameters E_ℓ' were defined to be:

$$E_\ell'(Zr) = -.529 \text{ Ry.} \quad \text{for } \ell = 0, 2, \ldots, 12, \text{ and}$$

$$E_\ell'(S) = -.529 \text{ Ry.} \quad \text{for } \ell = 0, 1, 2, \ldots, 12.$$

In order to avoid spurious roots (31) when $E'_{\ell=1}(Zr)$ was set to be -.529 Ry., the $E'_{\ell=1}(Zr)$ was given a different value (.20 Ry.).

The number of expansion coefficients of the eigenfunctions was truncated at 100. This value was determined from a convergence test of an eigenvalue of high contribution of d-states, with respect to the number of basis functions. Along the high symmetry directions, the eigenvalues were plotted versus the reduced wave vectors. This plot is shown in Fig. 3.1. With a formula unit, the average of 5 lowest energy bands were used to fill 10 valence electrons. The resultant Fermi level falls at .6829 Ry.

The energy bands were analyzed in terms of angular momentum quantum numbers (ℓ = 0, 1, 2, 3) of Zr and S by plotting the percentage of angular momentum contributions of the crystal wave functions inside the Zr and S muffin tin spheres, as shown in Figs. 3.2 and 3.3. The lowest band consists mainly of the sulfur-s states. As a result, it is usually called the s-band. The s-band is separated by a large gap (.53 Ry.) from the next three energy bands. In these three bands, the sulfur-p states yield the maximum contribution. In short, these bands are called the p-band. Then, after a narrow gap of .03 Ry., the next 5 energy bands

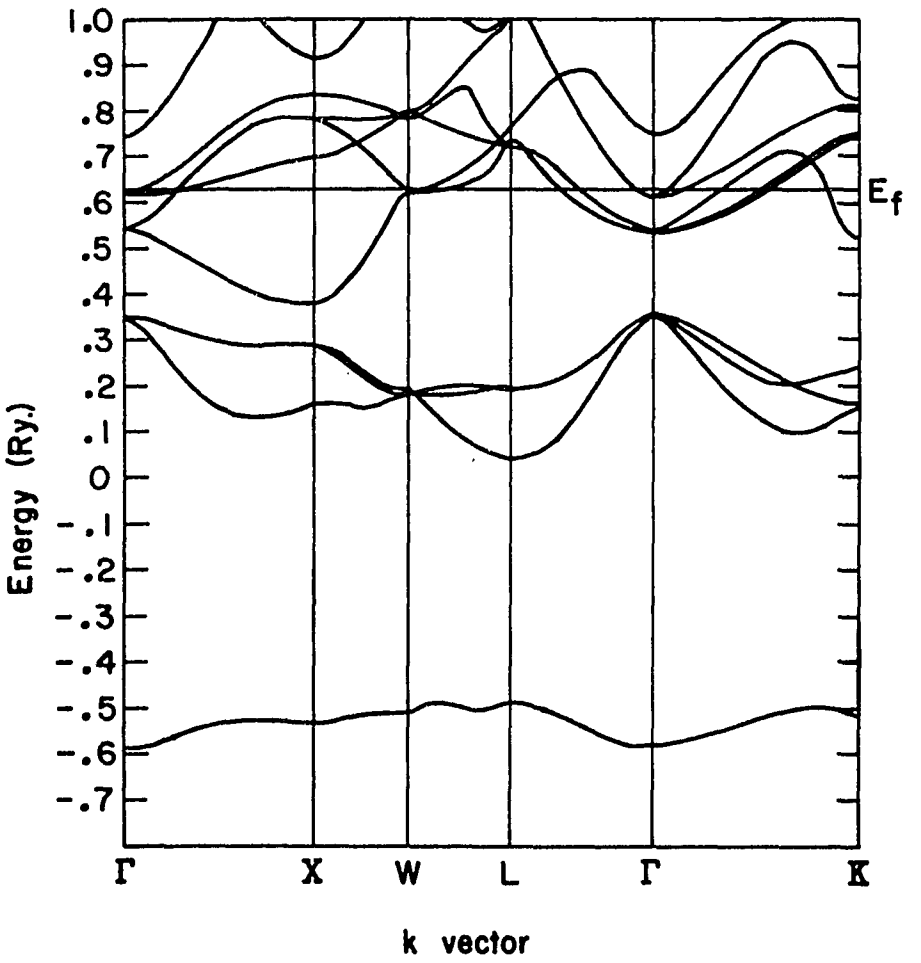

Fig. 3.1. Energy bands of ZrS (NaCl-type)

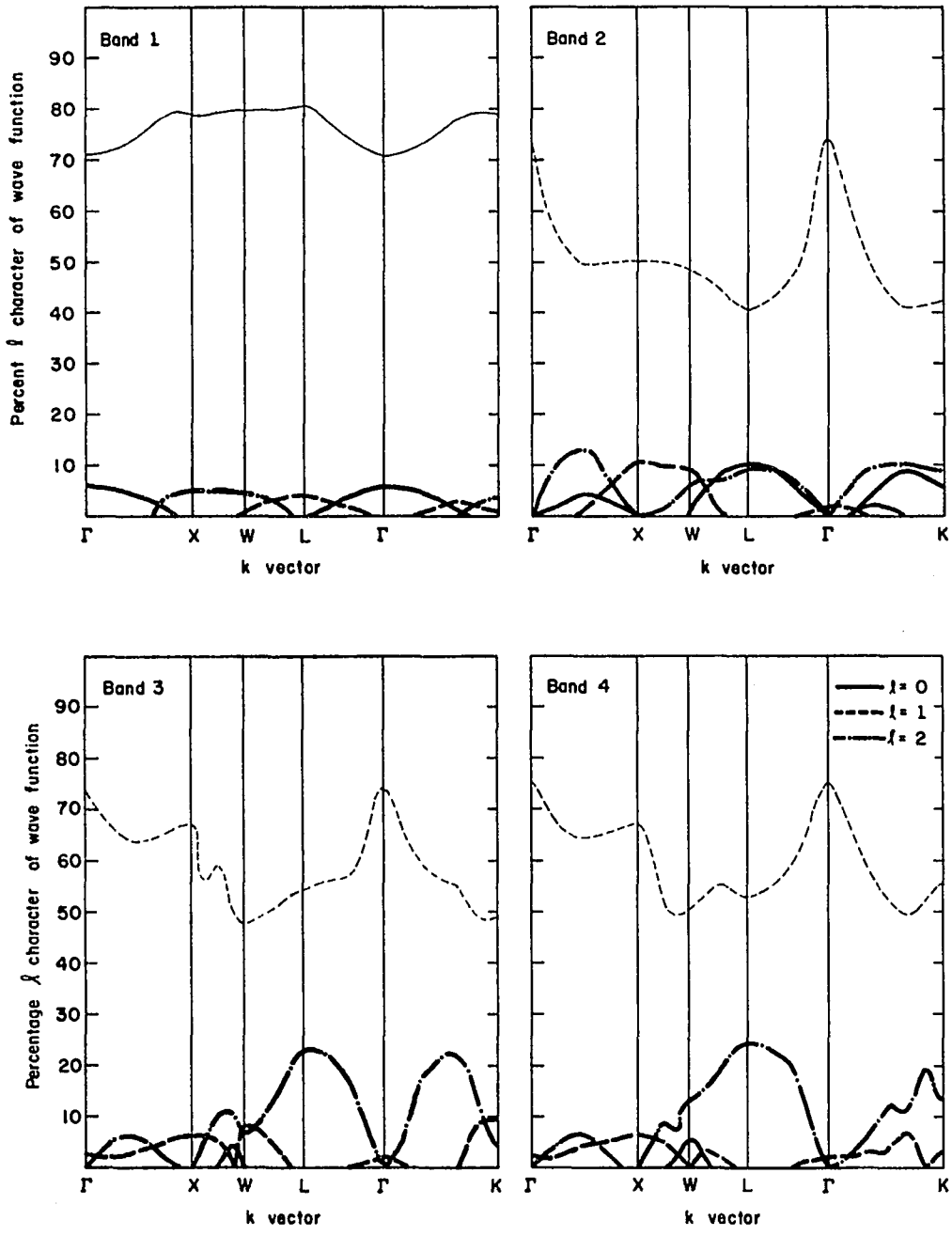

Fig. 3.2. ℓ-Decomposition of 1st-4th energy band of ZrS (NaCl-type) inside the Zr MT sphere (thick lines), and inside the S MT sphere (thin lines)

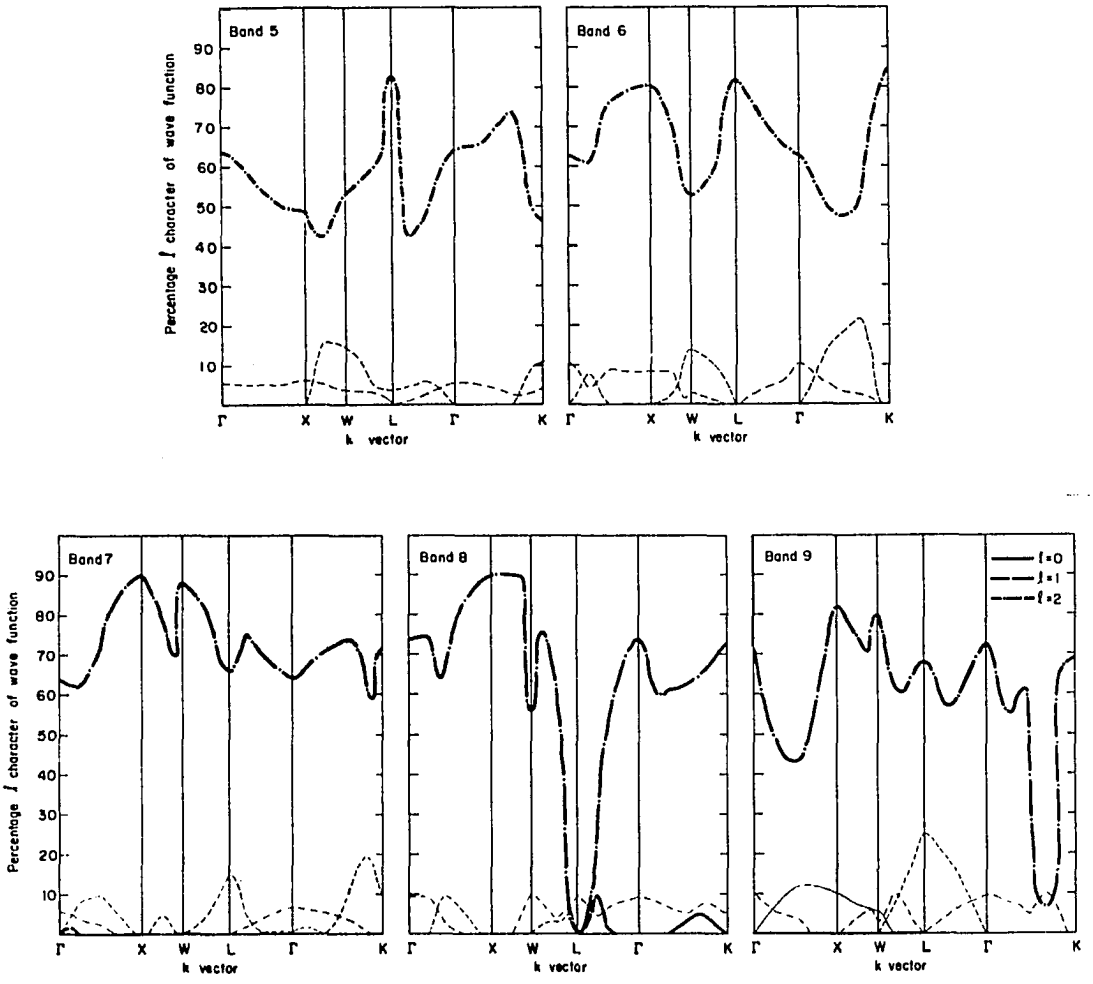

Fig. 3.3. ℓ-Decomposition of 5th-9th energy band of ZrS (NaCl-type) inside the Zr MT sphere (thick lines), and inside the S MT sphere (thin lines)

are mainly from zirconium d-states. Namely, the 5 bands are called the d-band.

The energy bands were fitted by a least squares method to a Fourier series which was truncated after the first 40 symmetrized plane waves. The Fourier coefficients were used to evaluate the energy bands at any arbitrary point in the Brillouin zone for use in calculating the density of states by the tetrahedron method. The root mean-square error of the fitted bands was within a few milli-Rydbergs.

For evaluating the density of states, the first Brillouin zone was divided into 2048 microtetrahedra. With the equations in Table 3.1 and equation 3.22, the density of states as well as its angular momentum decompositions, which are called the ℓ-partial density of states, were computed. They are shown in Fig. 3.4.

As shown in Fig. 3.4, the S-s states, S-p states and Zr-d states are the main contributions in the s band, p band and d band, respectively, as pointed out in Figs. 3.2 and 3.3.

The Zr-s states are observed to make only a small contribution in the occupied energy region, although the metal-s states are known to provide a broad occupied s band in the metal (32). The small contribution of the s states is interpreted to be a consequence of the interaction between Zr 5s and S 3s states resulting in a shifting of

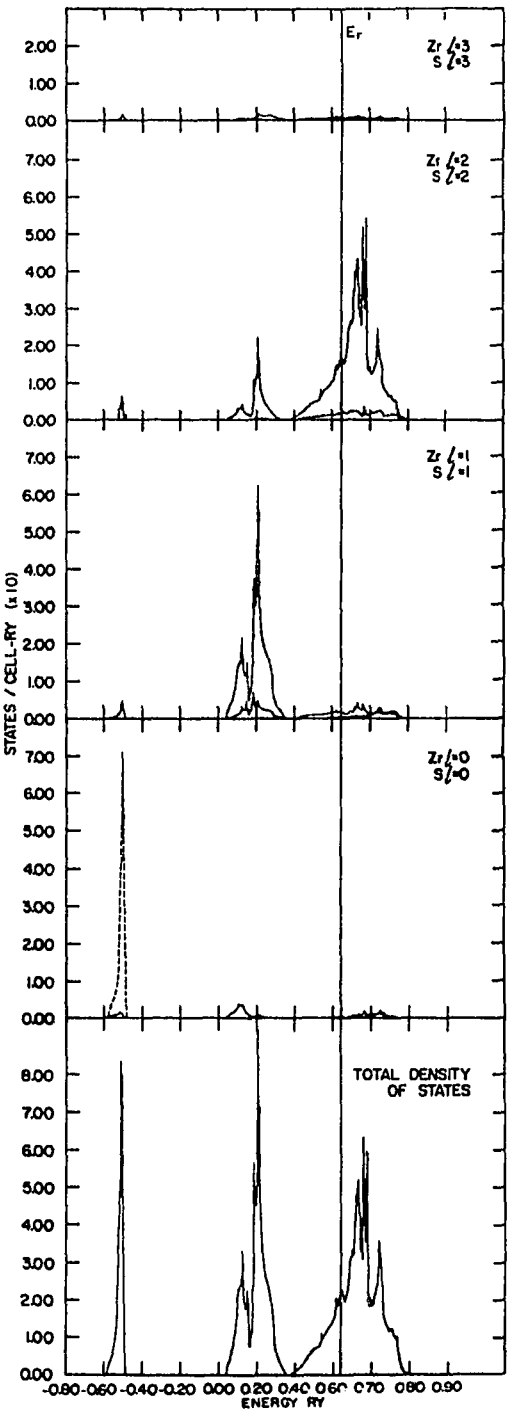

Fig. 3.4. Total DOS and angular momentum resolved DOS of ZrS, NaCl-type; (——: Zr, and ---: S in the resolved DOS)

Zr-s states to higher energy bands. This observation is also seen in the carbides, nitrides and oxides with the NaCl structure, as calculated by Neckel et al. (33), and is in agreement with the experimental evidence found by X-ray emission for the compound TiC.

TiC has the NaCl type structure in which the Ti atoms would be expected to a first approximation to have the same configuration as that of Zr atoms in ZrS with the NaCl structure type. As expected, Ramqvist and Manne (34) reported that no features from Ti 4s orbitals are observed in the X-ray spectra.

Further, the Zr d-partial density of states was divided into two contributions. One contribution includes the states d_{xy}, d_{yz} and d_{xz} symmetry called t_{2g}, which were found to contribute to the d bands and to a small extent to the p bands. The other contains the states of $d_{x^2-y^2}$ and d_{z^2} symmetry called e_g which make a small contribution to the s band and a recognizable contribution to the p bands and which for the most part are found in the unoccupied states of the d bands. As shown in Fig. 3.5, the results show a similarity with the e_g and t_{2g} contributions to carbides, nitrides, and oxides which have the NaCl structure as calculated using the APW method (35), or using a discrete variational method (36).

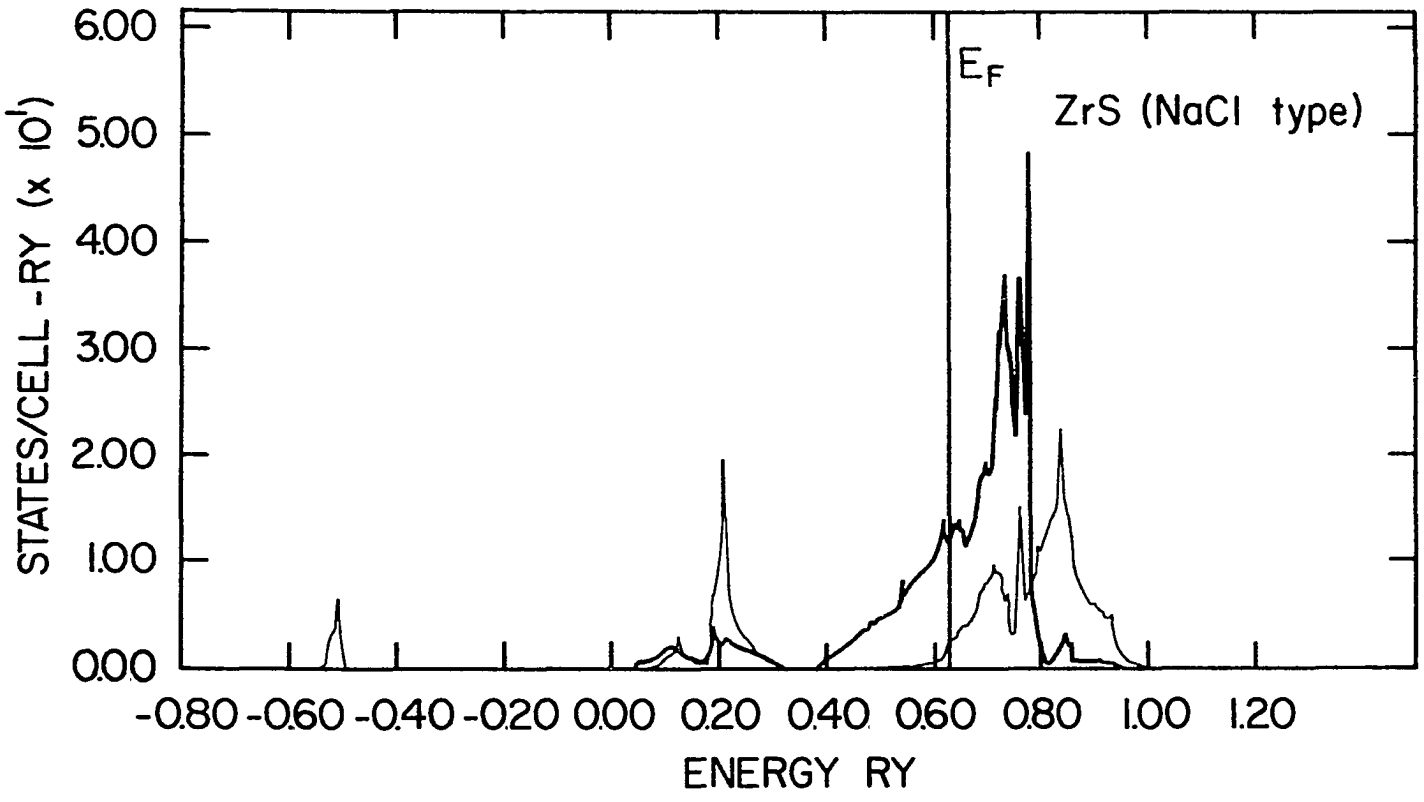

Fig. 3.5. Decomposition of Zr d-partial density of states into the t_{2g} (thick lines) and e_g (thin lines) contributions

Thus, the e_g-like states form bonding states in the p bands (as shown later), and so were pushed up to higher energy in the d bands.

To study directional bonding in ZrS with the NaCl structure type, the average value of the square of the crystal wave functions ($\psi^*\psi$) inside the muffin tin spheres (called charge density or electronic distribution) was computed. The charge densities were also calculated using the eigenfunctions corresponding to energies in different energy ranges. The results are represented by the charge densities, evaluated in the 100 plane, passing through the center of the muffin tin spheres. Table 3.3 lists the figure numbers and their corresponding contents, concerning the charge densities of the Zr and S muffin tin spheres.

Table 3.3. Charge densities inside the MT spheres of ZrS NaCl-type

Figure number	Sphere	Energy range
3.6a	Zr	s band
3.6b	Zr	p bands
3.6c	Zr	occupied d bands
3.7a	S	p bands
3.7b	S	occupied d bands

As shown in Figs. 3.6a and 3.6b, the charge density maxima at the Zr muffin tin sphere boundary are pointed directly to the sulfur atoms (the relative position of Zr and S atoms on the 100 plane is found in Fig. 3.8). These results indicate that the orbitals centered on the Zr atoms from the s and p band states were used in σ bonding to the sulfur atoms. It is also demonstrated in Fig. 3.5 that the e_g-like states of Zr are located in the s band and in the p bands.

On the other hand, in the occupied d bands the charge density at the sphere boundary is maximized along the Zr-Zr directions, as shown in Fig. 3.6c. The number located along the Zr-Zr direction is the value of the charge density (el/a.u.^{3}), evaluated at the intersecting point of the sphere boundary and the line connecting the Zr with one of the nearest neighbor Zr sites. This number will be used as a guideline for a comparison of metal-metal interactions in ZrS for the NaCl-type structure and for the WC-type structure. The metal-metal interaction is also shown (Fig. 3.5), by the large contribution of t_{2g}-like states of Zr in the occupied d bands.

The t_{2g}-like states of Zr were also detected in the p bands, but made a small contribution compared with the e_g-like states. As a consequence of small contribution in the p bands, the charge density for the p bands along the Zr-Zr direction is significantly smaller than the charge density along the Zr-S direction, as shown in Fig. 3.6b.

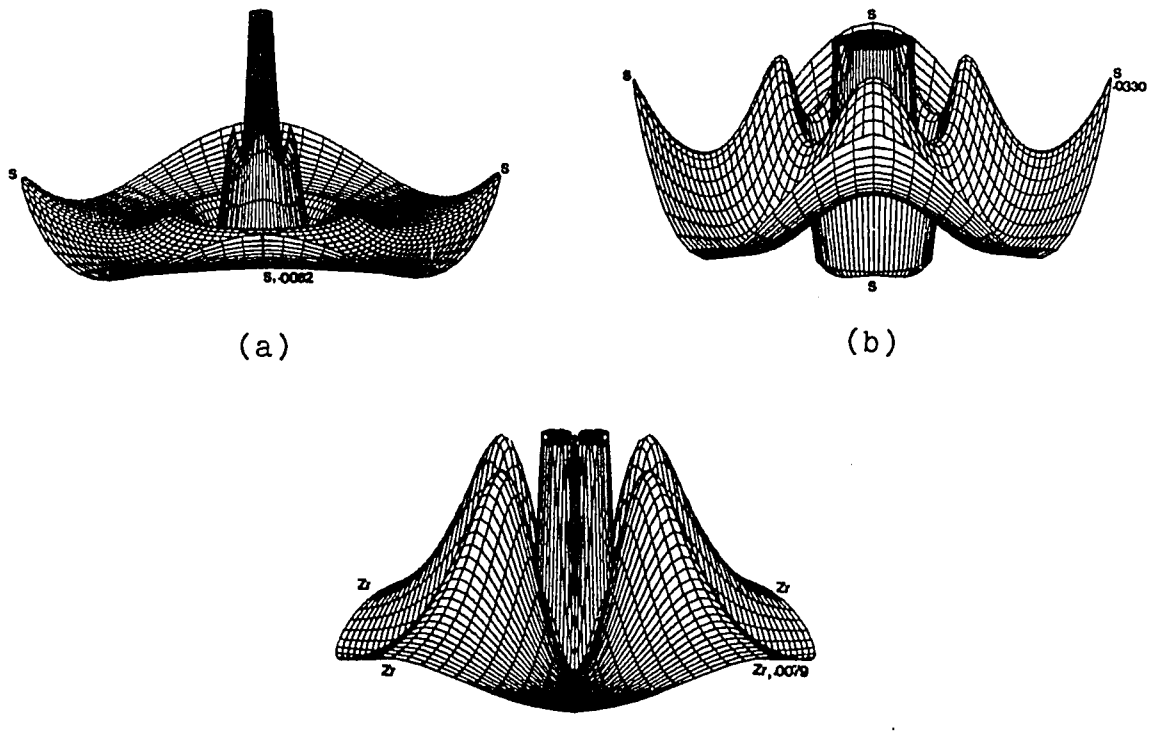

Fig. 3.6. Charge density in the plane 100 inside the Zr MT sphere; (a) includes all the states in the s band, (b) includes all the states in the p bands, and (c) includes the occupied states within the d bands

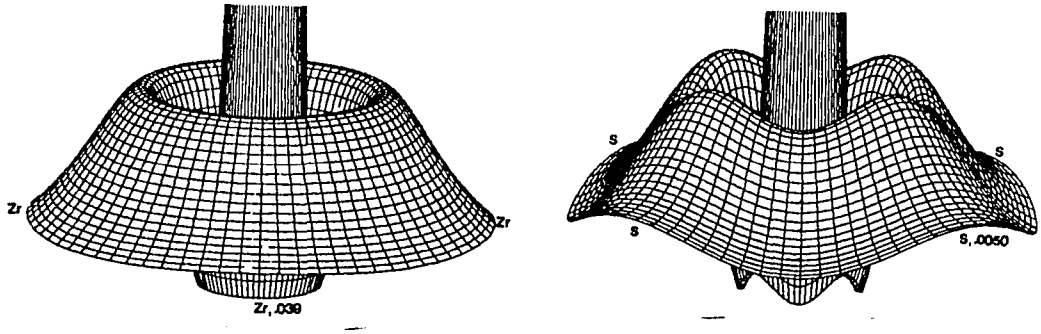

(a) (b)

Fig. 3.7. Charge density in the plane 100 inside the S MT sphere; (a) includes the states in the p bands, (b) includes the states in the occupied d bands

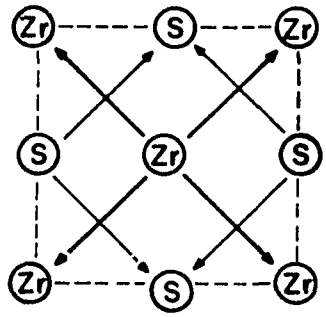

Fig. 3.8. Schematic diagram of charge densities of Zr and S MT spheres, for the states in the occupied d bands, in the plane 100 of ZrS NaCl-type

As opposed to the charge densities shown in the Zr MT spheres, the charge densities inside the S MT spheres in the p bands (Fig. 3.7a) and in the s band (not shown) are essentially spherically symmetric. They are not so useful in explaining the bonding directions in the structure. In the occupied d bands, the small charge density inside the S MT spheres is shown to maximize in the direction toward another sulfur atom at the centers of the faces of the cubic unit cell. The schematic diagram of directions of the charge densities inside the Zr and S MT spheres on the 100 plane is shown in Fig. 3.8.

In summary, the directions of the charge density maxima at the boundary of the Zr and S MT spheres can be used to express the interatomic interactions in the ZrS NaCl-type in the following way.

In the energy interval of the s band and the p bands, the charge density in the Zr MT sphere boundary is maximized along the Zr-S direction, and indicates direct interactions between Zr and S atoms via σ bonding. This observation can be interpreted as resulting from covalent bonding in ZrS with the NaCl structure. As shown in Fig. 3.9, by joining the charge density of Zr and S MT spheres along the 100 direction, the charge density is shown to share between two atomic sites Zr and S in a manner characteristic of covalent bonding. In the

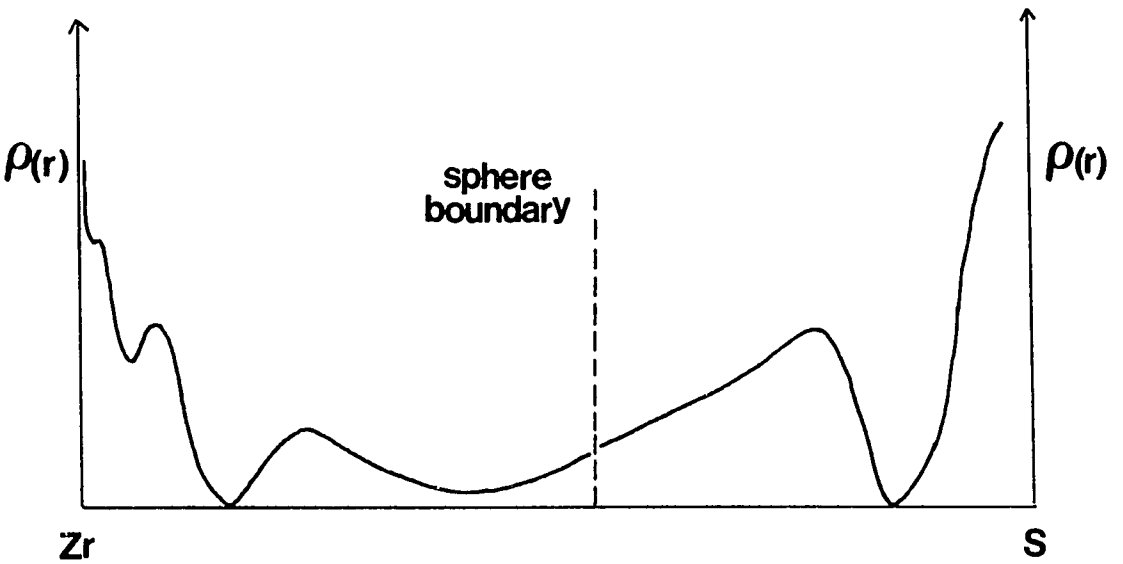

Fig. 3.9. Charge densities of Zr and S MT spheres along the direction 100

occupied d bands, the charge density at the Zr MT sphere boundary points toward the nearest neighbored Zr sites resulting from metal-metal bonding via σ interactions, and from metal-nonmetal bonding via π interactions. Besides the covalent bonding and metal-metal bonding, ionic bonding in terms of charge transfer is usually associated with compounds with the NaCl structure. Unfortunately, the non-self-consistent calculation would not give a meaningful value for charge transfer. Therefore, the ionic character of ZrS with the NaCl structure was examined by a photo-electron spectroscopy study, and will be discussed in Chapter IV.

3. ZrS WC-type

ZrS of WC structure crystallizes with a space group D^1_{3h}, which corresponds to a hexagonal lattice. Utilizing 12 symmetry operations of the D^1_{3h} space group, it is only necessary to evaluate eigenvalues and eigenfunctions at k points within one twelfth of the first Brillouin zone. Furthermore, because of the symmorphic nature of the space group D^1_{3h}, time-reversal symmetry can cause extra degeneracies (37). That is, $E(k)=E(-k)$ for all k. As a consequence, the first Brillouin zone was divided into twenty-four equivalent triangular prisms. The eigenvalues and eigenfunctions were evaluated at 63 k points distributed evenly in one twenty-fourth of the first Brillouin

zone, and at 58 k points along the high symmetry lines of the one twenty-fourth zone. The 63 k points were located in 7 planes stacking along $\frac{c^*}{2}$ (c^* = reciprocal lattice vector of the hexagonal c axis) of the triangular prism. Then, at each plane there are 9 k points selected at centers of 9 triangles, fit inside each plane.

At each selected k point, at least 9 eigenvalues and the corresponding eigenfunctions were evaluated. To determine the eigenvalues and eigenfunctions as accurately as possible, the energy parameter E' in equation (3.3) was chosen separately for each energy range. For positive eigenvalues, the energy parameter E' at zirconium sites and at sulfur sites were defined as:

$$E'_{\ell}\ (Zr) = .50 \text{ Ry.} \qquad \text{for } \ell = 0, 1, \ldots, 12, \text{ and}$$

$$E'_{\ell}\ (S) = .35 \text{ Ry.} \qquad \text{for } \ell = 0, 1, \ldots, 12.$$

For the negative eigenvalues, the energy parameters E' were defined differently:

$$E'_{\ell}\ (Zr) = -.520 \text{ Ry.} \qquad \text{for } \ell = 0, 2, \ldots, 12, \text{ and}$$

$$E'_{\ell}\ (S) = -.520 \text{ Ry.} \qquad \text{for } \ell = 0, 1, \ldots, 12.$$

Similar to the previous calculation, the energy parameter $E'_{\ell=1}\ (Zr)$ was given a value 0.0 Ry. to avoid spurious roots. As a result of a convergence test of an eigenvalue containing a high percentage of d states, relative to the number of basis functions, the number of expansion

coefficients in equation (3.8) was cut off at 120, slightly higher than in the previous calculation.

Along the high symmetry directions, the eigenvalues were plotted versus the reduced wave vectors. This result is shown in Fig. 3.10. As was the case for ZrS with NaCl structure type, an average of 5 occupied energy bands is required for 10 valence electrons of ZrS. Thus, the Fermi energy was determined to be at .560 Ry.

The 9 energy bands at lower energies were analyzed to yield the percentage of angular momentum contribution of the wavefunctions along the high symmetry directions for each band, as shown in Figs. 3.11 and 3.12. Again, for the same reasons mentioned in the previous calculation, the lowest band is called the s band. The following three bands, in short, are called the p band, and the last 5 bands are the d band.

By the same method used in the previous calculation for evaluating the density of states and the angular momentum decomposition of density of states, the energy bands were fitted with 50 Fourier coefficients, using the least squares method. The root mean square error of the fitting for each band was on the order of a few milli-Rydbergs. The results of density of states and ℓ-partial density of states are shown in Fig. 3.13.

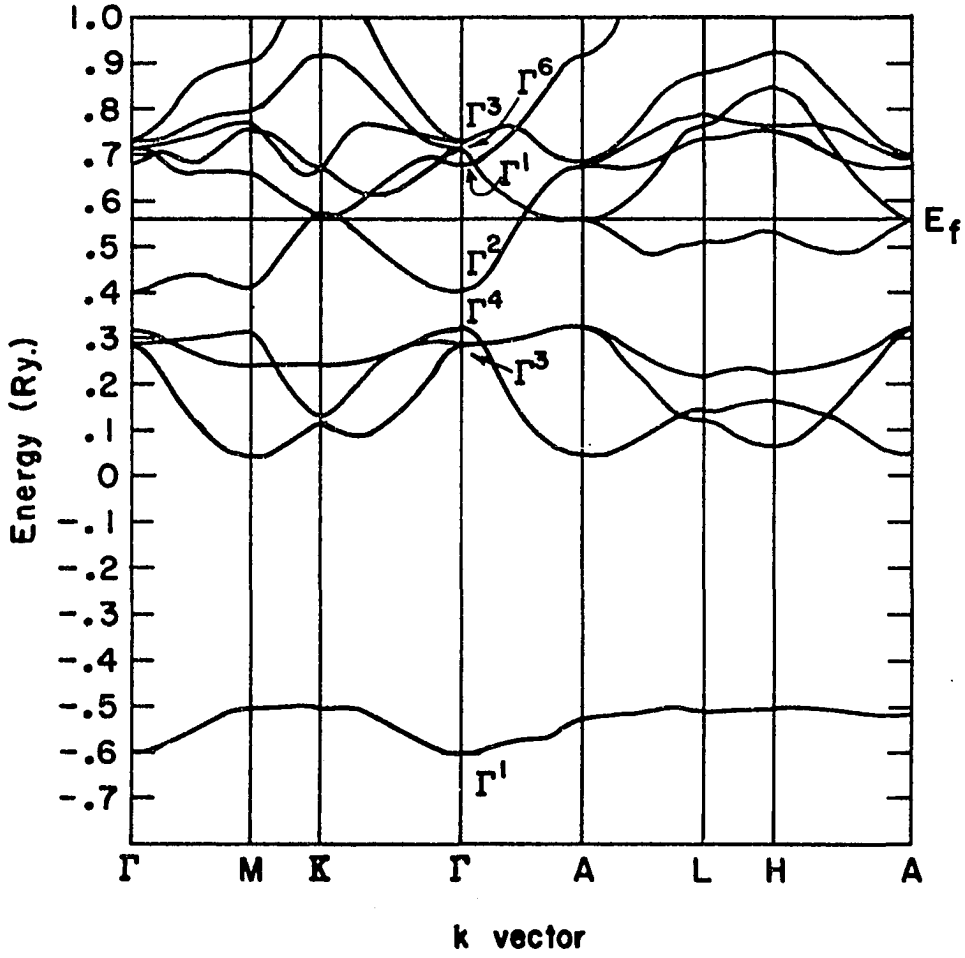

Fig. 3.10. Energy bands of ZrS (WC-type). (The symmetry representations at Γ point are obtained from Ref. 37)

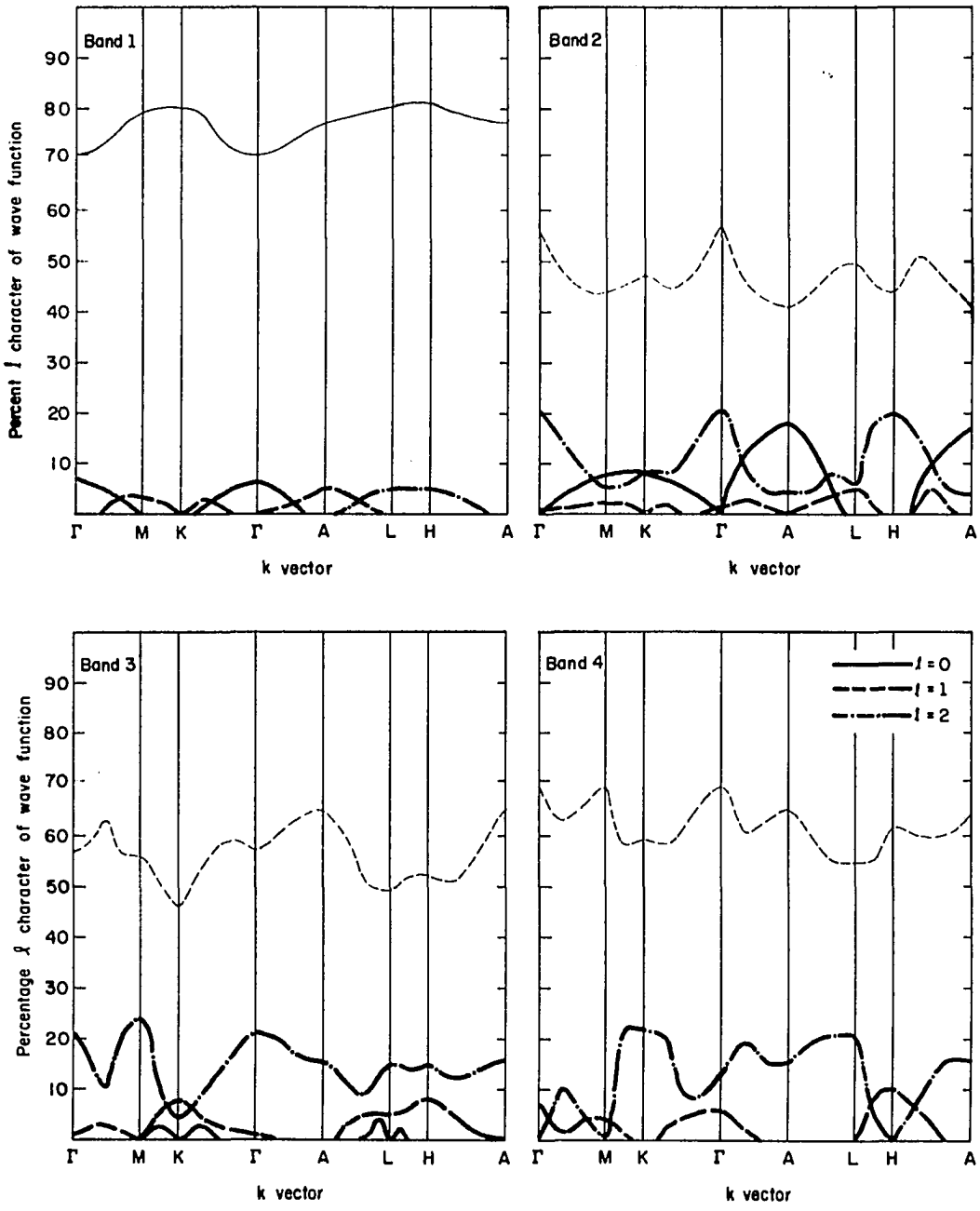

Fig. 3.11. ℓ-Decomposition of 1st-4th energy band of ZrS (WC-type) inside the Zr MT sphere (thick lines) and inside the S MT sphere (thin lines)

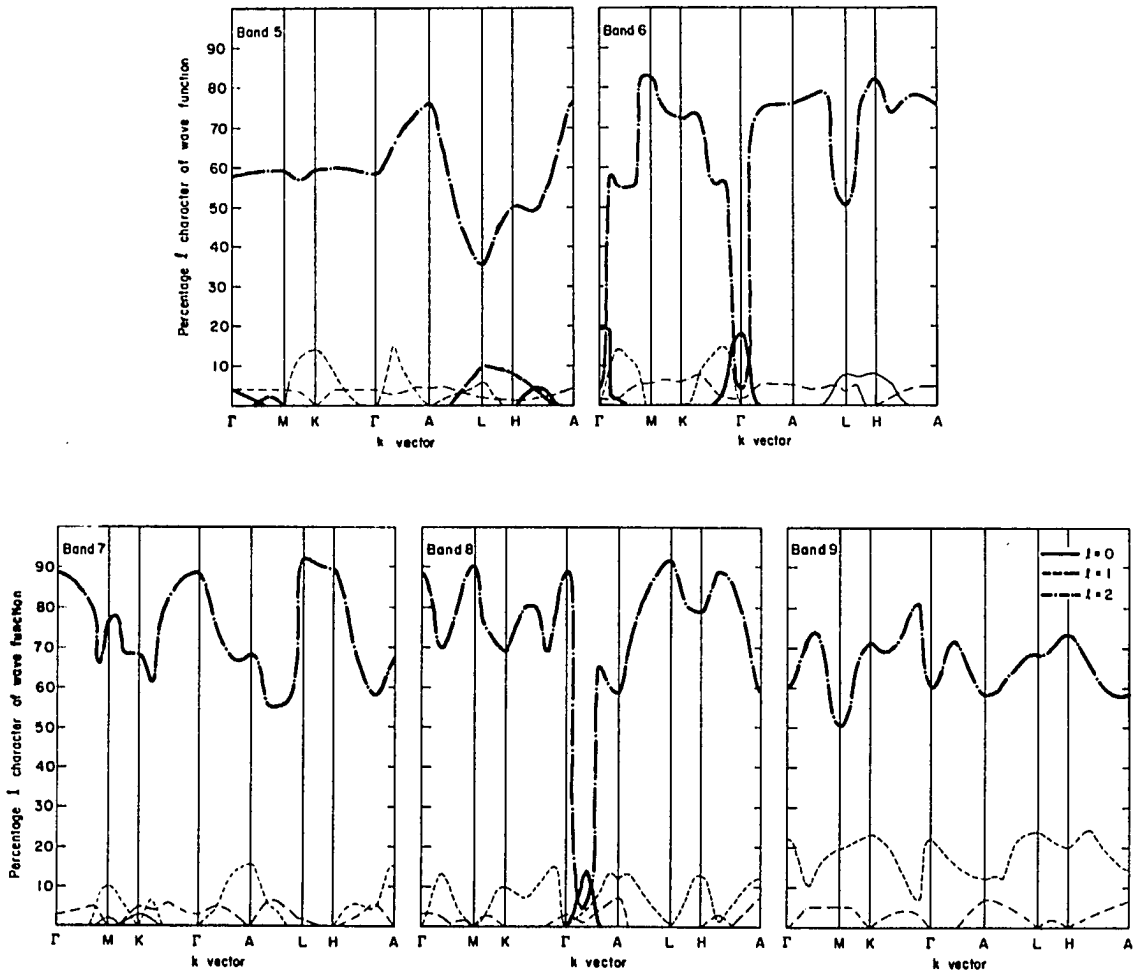

Fig. 3.12. ℓ-Decomposition of 5th-9th energy band of ZrS (WC-type) inside the Zr MT sphere (thick lines) and inside the S MT sphere (thin lines)

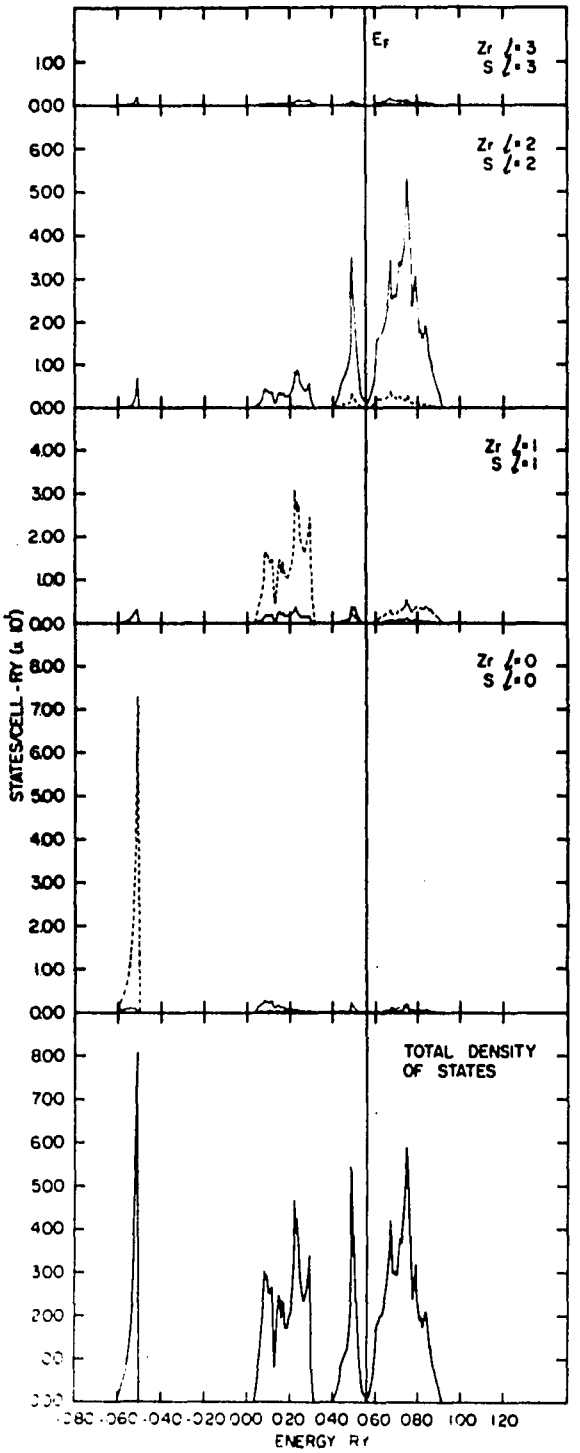

Fig. 3.13. Total DOS and angular momentum resolved DOS of ZrS, WC-type; (——: Zr, ---: S in the resolved DOS)

To investigate the directions of bonding, the charge density was computed. The charge density was evaluated in various planes passing through the center of the muffin tin spheres, i.e., the xy plane, the yz plane, and the xz plane. The following table, Table 3.4, lists the figure numbers and the information presented in each figure.

Figure 3.4. Charge densities inside the MT spheres of ZrS WC-type

Figure number	Sphere	The plane in which the charge density is displayed	Energy range
3.14a	Zr	yz	s band
3.14b	Zr	xy	s band
3.14c	Zr	xz	s bands
3.15a	Zr	xz	p bands
3.15b	Zr	yz	p bands
3.15c	Zr	xy	p bands
3.16a	Zr	yz	occupied d bands
3.16b	Zr	xy	occupied d bands
3.16c	Zr	xz	occupied bands
3.17a	S	yz	occupied d bands
3.17b	S	xy	occupied d bands
3.17c	S	xz	occupied d bands
3.17d	S	xz	p bands

In the s band, with the main contribution of sulfur s states, the charge densities of Zr MT spheres show that besides the direct Zr-S interactions, there was some charge build-up along $\vec{x}$, $\vec{x}'$ and $\vec{x}''$ directions (see Figs. 3.14b and 3.14c), although the charge maximum at the sphere boundary along the $\vec{x}$, $\vec{x}'$ and $\vec{x}''$ directions (.0004 el/a.u.^{3}) was less than the charge oriented toward the sulfur atoms (.0009 el/a.u.^{3}).

On the other hand, only the direct Zr-S interactions between Zr atoms and S atoms could be detected in the p bands (e.g., see Figs. 3.15a-c representing the hybridized sulfur p states and zirconium d states).

Moving on to the occupied d bands containing mostly the Zr d states, Fig. 3.16a shows that between the metal atoms, the interactions in the plane are more important than the interactions along the c axis. However, as shown in Figs. 3.16b and 3.16c, the charge was concentrated even more along the $\vec{x}$ axis, and equivalently along the $\vec{x}'$ and $\vec{x}''$ directions. The net charge of Zr atoms along the three directions $\vec{x}$, $\vec{x}'$ and $\vec{x}''$ is represented by the arrows, and shown in Fig. 3.18. This charge distribution is referred to as a three-center bond.

In summary, the metal-metal interactions are stronger in the xy plane than along the direction normal to the plane. Therefore, with this observation, the electrical conductivity of ZrS with the WC structure would be expected

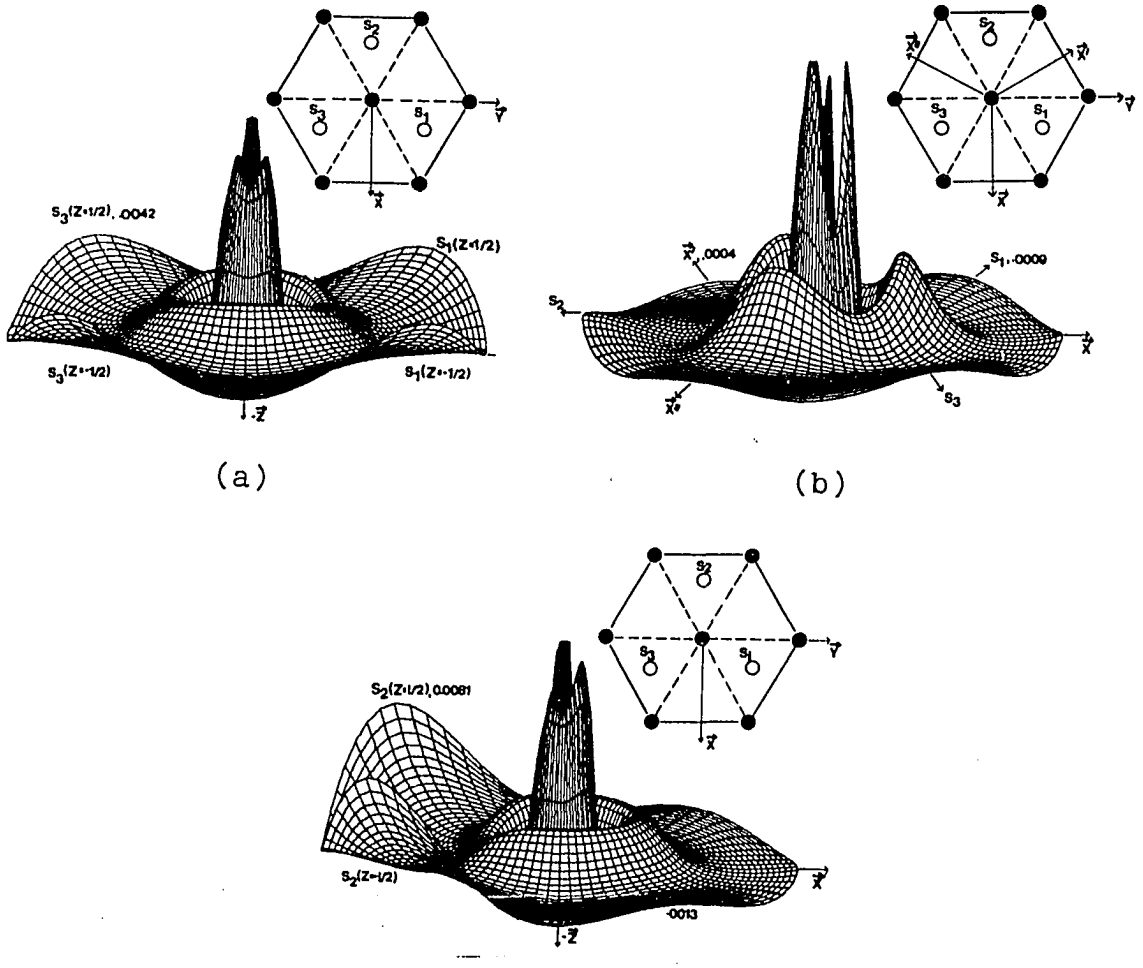

Fig. 3.14. Charge density inside the Zr MT sphere includes all the states in the s band (a) in the yz plane; (b) in the xy plane; (c) in the xz plane

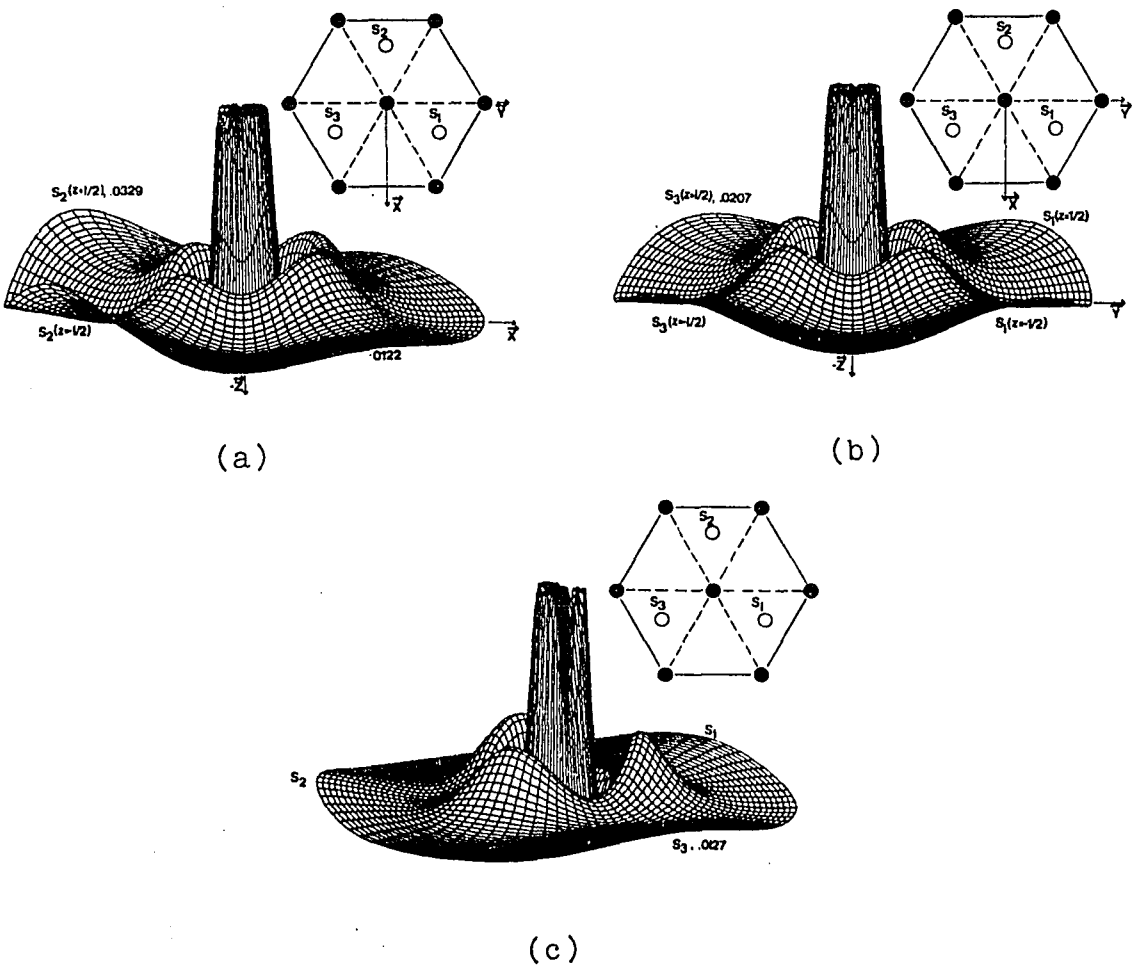

(a) (b)

(c)

Fig. 3.15. Charge density inside the Zr MT sphere includes all the states in the p bands (a) in the xz plane; (b) in the yz plane; (c) in the xy plane

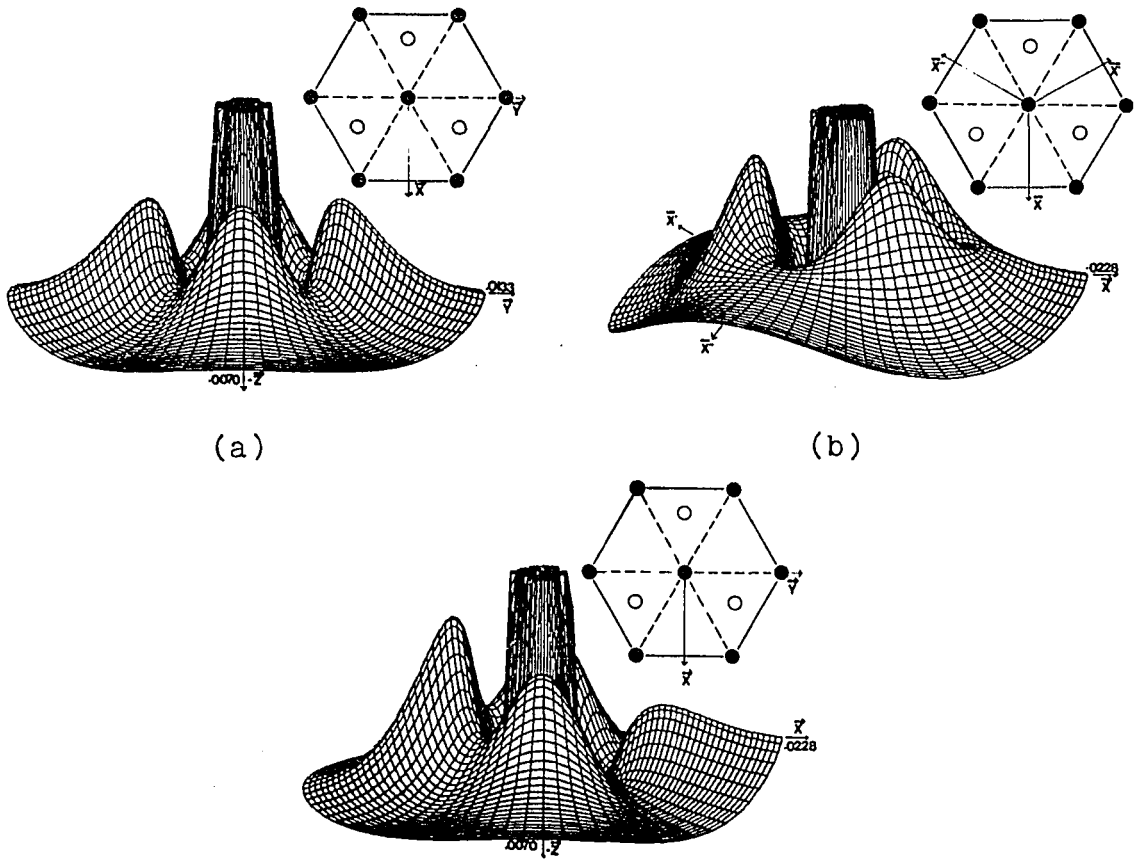

(a) (b)

(c)

Fig. 3.16. Charge density inside the Zr MT sphere includes all the states in the occupied d bands (a) in the yz plane; (b) in the xy plane; (c) in the xz plane

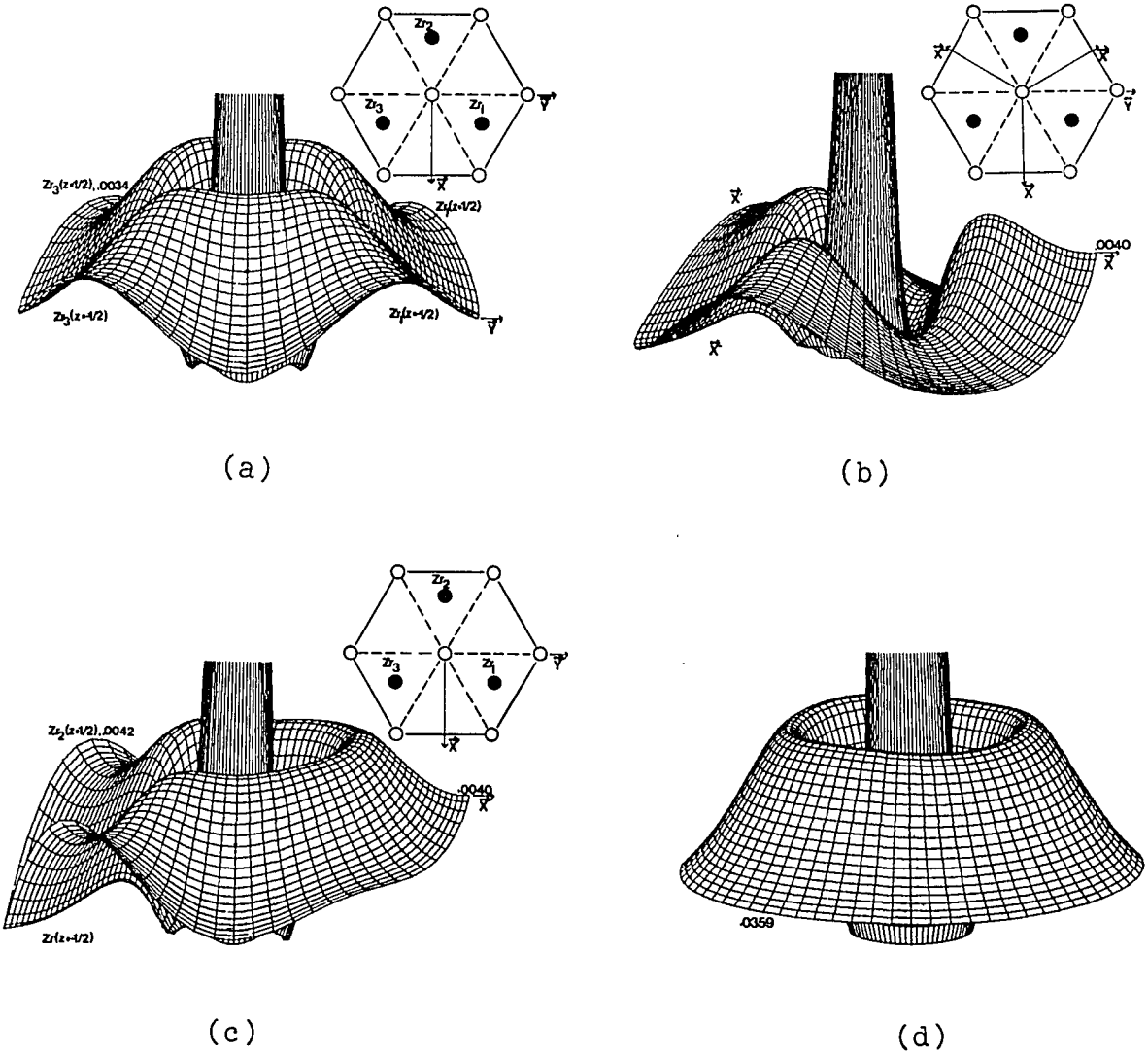

Fig. 3.17. Charge density inside the S MT sphere includes all the states in the occupied d bands (a) in the yz plane; (b) in the xy plane; (c) in the xz plane; and includes all the states in the p bands (d) in the xz plane

to show an anisotropic behavior, having a higher electrical conductivity in the plane than along the c axis.

In contrast to the charge densities displayed by the Zr MT spheres, the charge densities of the S MT spheres from the p bands (3.17d) and from the s band (not shown) are essentially spherically symmetric. Therefore, they are not useful in discussion about the directional bonding. However, in the occupied d bands, Fig. 3.17b again shows that the charge is oriented along the $\vec{x}$, $\vec{x}'$ and $\vec{x}''$ directions. The net charge of sulfur on the xy plane could also be represented by Fig. 3.18.

In the combination of the charge created by the Zr atoms and by the S atoms on the xy planes, by stacking the xy plane of Zr atoms and the xy plane of S atoms as in the WC structure, the charge was found to locate along the empty channel of the structure, and it is shown in Fig. 3.19. Besides the charge oriented along the $\vec{x}$, $\vec{x}'$ and $\vec{x}''$ directions, the sulfur atoms also indicate some interactions with zirconium atoms as shown in Figs. 3.17a and 3.17c. However, these interactions are much smaller than the Zr-Zr interactions. Therefore, these features are wiped out by the overwhelming charge density along the metal-metal directions and along the $\vec{x}$, $\vec{x}'$ and $\vec{x}''$ directions in Figs. 3.16a-c.

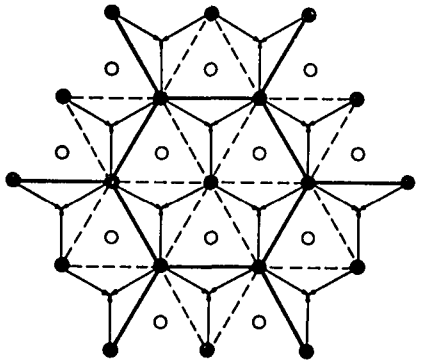

Fig. 3.18. Three-center bond

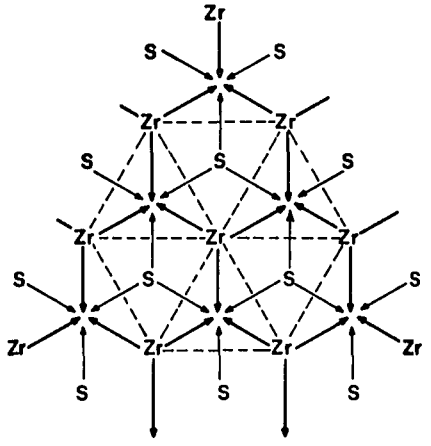

Fig. 3.19. Schematic diagram of charge distribution of ZrS, WC-type in the occupied d bands

Using the directions given by the maxima in the charge densities evaluated inside the Zr and S muffin tin sphere, the nature of bonding in ZrS with the WC structure is expressed in the following way. States in the s band and p bands yield a charge density in the Zr sphere which is pointing directly toward the sulfur atoms indicating a covalent contribution to the Zr-S bonding in the ZrS with the WC structure, as demonstrated in ZrS with the NaCl structure. From the directions of charge density maxima displayed within the Zr muffin tin sphere, and the ℓ-partial density of states calculated for the s band and p bands, the interactions between the Zr and S atoms are assumed to arise from the overlap of Zr d_{xz} and d_{yz} orbitals with sulfur s orbitals in the s band; and from the overlap of Zr d_{xz} orbitals with sulfur p_x and p_z orbitals, and from the overlap of Zr d_{yz} orbitals with sulfur p_y and p_z orbitals in the p bands. (The direction of the orbitals is referred to as Cartesian coordinates XYZ, as shown in Fig. 3.15a.)

Furthermore, in the s band the charge density maxima within the Zr muffin tin sphere show a three-center bond similar to that shown by the charge density inside the Zr muffin tin sphere by states in the occupied d bands. However, the charge density at Zr muffin tin sphere boundary, pointing to the three-center bond is much smaller in the

s band (.0004 el/a.u.^{3}) than in the case of the occupied d bands (.0228 el/a.u.^{3}). This observation is also illustrated by the Re_3Cl_9 molecule in which the three-center bond is formed inside the triangle of three Re atoms (38).

In the occupied d bands, besides the charge density at the muffin tin sphere boundary which is maximized in the directions of the three-center bond, the charge density also shows reasonably high values along the metal-metal direction in the xy plane (.0133 el/a.u.^{3}), and along the metal-metal direction along the z axis (.0070 el/a.u.^{3}). The direct interactions between metal atoms in the xy plane as well as along the z axis can be explained on the basis of overlap of neighboring d_{xy}-d_{xy} orbitals and d_{z^2}-d_{z^2} orbitals, respectively.

The charge density in the S muffin tin sphere, including all the states in the occupied d bands, also indicates the existence of Zr-S interactions, although they are the weak interactions when compared with the metal-metal interactions in the occupied d bands. The charge density of sulfur also demonstrates features of the three-center bond which might result from the small population of sulfur-d states in the occupied d bands.

In conclusion, among the five d orbitals of Zr atoms, the orbitals $d_{x^2-y^2}$, d_{xy} and d_{z^2} are involved in the

metal-metal interactions; and the d_{xz} and d_{yz} orbitals are utilized in the metal and nonmetal interactions with the p_x, p_y and p_z orbitals of the sulfur atoms.

This conclusion for metal-metal interactions is found to be comparable with the conclusion made by England et al. for metal-metal interactions in VS with the NiAs structure (39). The $d_{x^2-y^2}$, d_{xy} and d_{z^2} orbitals are involved in metal-metal bonding for the compound VS in which V atoms have antitrigonal prismatic coordination and S atoms have trigonal prismatic coordination.

Besides the Zr-S covalent bonding and the Zr-Zr metal bonding, ionic bonding is usually also considered for a compound. The ESCA results of this work indicate a small but observable contribution of ionic bonding in ZrS. However, the nonself-consistent calculations do not give an accurate value for charge transfer. Therefore, the discussion about the ionic character of ZrS with the WC structure in terms of charge transfer will be delayed until Chapter IV.

4. Bonding comparison between ZrS NaCl-type and ZrS WC-type

As stated above, covalent interactions are found for both structure types in the s band and p band regions, as demonstrated by the charge shared between two atomic sites. The charge density in the p bands at the sulfur MT sphere boundary was found to be .0390 (el/a.u.^{3}) along the Zr-S

direction in ZrS with the NaCl structure, and was found to be .0359 (el/a.u.^{3}) along the Zr-S direction in ZrS with the WC structure. These values indicate that the covalent contribution to bonding is equally important in both structure types, a result which correlates well with the similarity of Zr-S distances in both structures, e.g., d = 2.580 Å for the NaCl structure, and d = 2.627 Å for the WC structure.

As discussed above, metal-metal bonding is also exhibited by the two structure types, although the metal-metal interactions are more important in the WC structure than in the NaCl structure. As shown in Figs. 3.16a-c, the charge density in the occupied d bands at the Zr muffin tin sphere boundary is .0228 (el/a.u.^{3}) along the three-center bond directions, .0133 (el/a.u.^{3}) along the metal-metal direction in the xy plane, and .0070 (el/a.u.^{3}) along the z axis for ZrS with the WC structure. However, for ZrS with the NaCl structure, the charge density in the occupied d-bands at the Zr MT sphere boundary maximizes with a value .0079 (el/a.u.^{3}) along the Zr-Zr direction. This observation correlates well with the shorter metal-metal distance in the WC structure and with the reduction of the number of nearest neighbor metal atoms from the NaCl structure (12) to WC structure (≈8). The decrease in metal-metal distance yields an increased overlap of occupied metal orbitals, as

demonstrated by the overlap of the radial parts of Zr d orbitals at the metal-metal distance in the NaCl-type structure compared with that in the WC structure (Fig. 3.20).

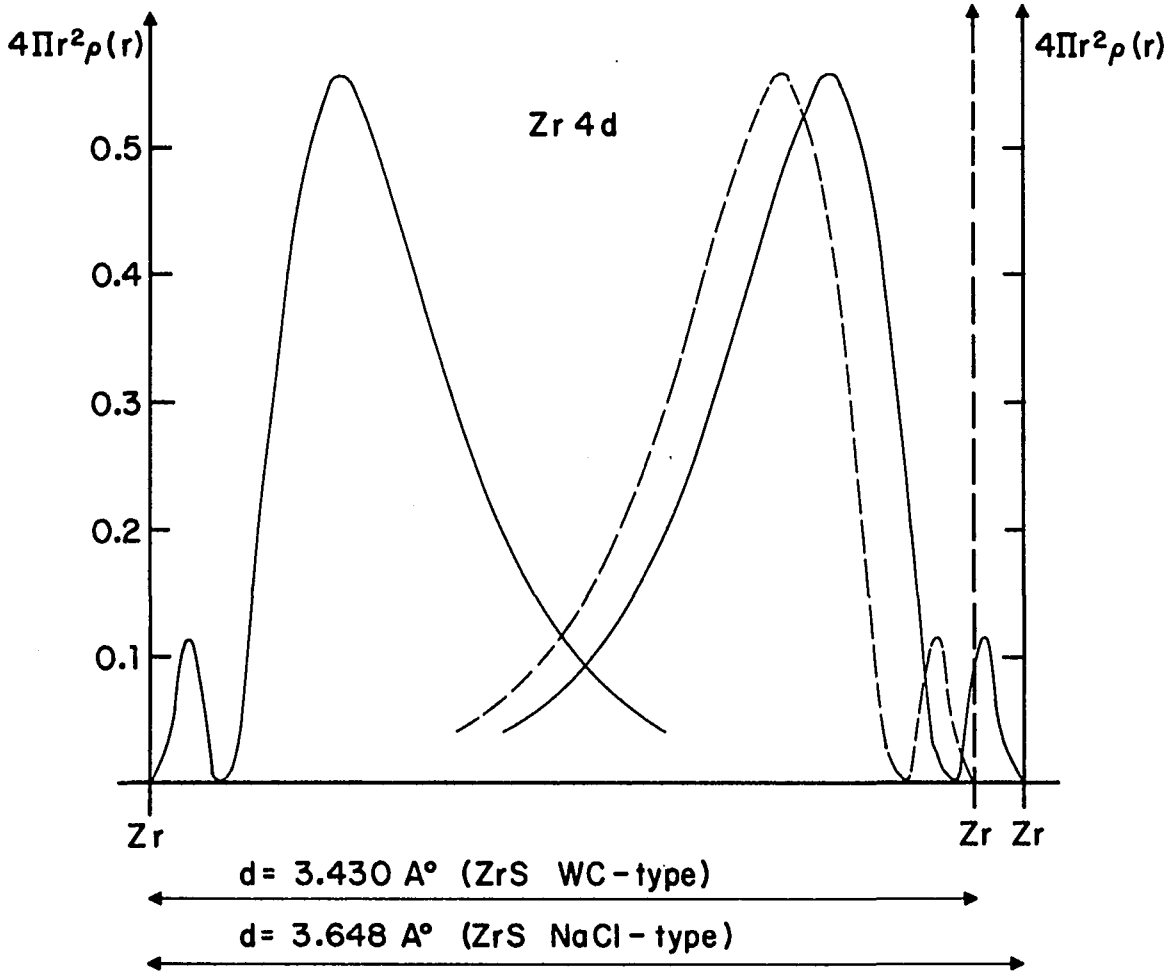

Fig. 3.20. Overlap of atomic radial part of Zr 4d orbitals along Zr-Zr direction in ZrS (NaCl-type) and in ZrS (WC-type)

IV. PHOTOELECTRON SPECTROSCOPY

A. Introduction

Since the mid-1960s, ESCA (Electron Spectroscopy for Chemical Analysis) has become a powerful tool for scientists. One kind of valuable information that ESCA provides is the qualitative charge transfer in binary or higher compounds. By measuring the kinetic energies of electrons exiting from specified levels of materials as the result of bombardment with an X-ray beam of known energy, the binding energies can be calculated. These binding energies reflect how tightly the electrons are bound to the nuclei, and thus because of the chemical shift in the binding energies, information about the direction of charge transfer in the samples is given. Furthermore, the photoelectron spectra of low binding energies, about 0-20 eV below the fermi energy, called the valence band spectra, resemble the calculated density of states. Utilizing the information given by ESCA, the binding energies of Zr 3d and S 2p core levels, and the valence band spectra of ZrS_{1+x} and ZrS_{1-x} were measured.

B. Experiment

The Zr-S samples were put into a glove box, attached directly to the sample port of an AEI ESCA 200B photoelectron

spectrometer. The glove box was filled with continuously purified helium to maintain the O_2 and H_2O levels below 1 ppm and .5 ppm, respectively. After being ground with mortar and pestle, the powdered samples were pressed into a piece of indium foil attached to a silver backing. The silver provided the binding energy of Ag $3d_{5/2}$ as an internal standard to calibrate the spectrometer. The Ag pieces, carrying the indium foil with pressed samples, were mounted on the sample probe of the spectrometer and inserted into the spectrometer. During the measurements, the residual pressure of the sample chamber was less than 1×10^{-8} torr as measured by a calibrated hot cathode ionization gauge. Measurements were made with unmonochromatized Al K_α radiation ($h\nu$ = 1486.6 eV), and with the narrowest slits. The data were collected by signal averaging over the core level and the valence band regions by using a Nicolet 1180 computer. Typically, the core levels of Zr 3d and S 2p of the Zr-S samples were scanned for 20 and 30 scans over 12.5 eV range, respectively. For the valence bands, the spectra were signal averaged from 350 scans over a 25 eV range.

The ZrS_{1+x} and ZrS_{1-x} samples are known to show metallic behavior (5), therefore charging problems were not encountered in this study.

The results will be listed in a following section without the correction for lattice site potential (40).

C. Results and Discussion

The binding energies of Zr 3d and S 2p levels in Zr-S compounds with a variety of compositions were measured and are listed in Table 4.1, along with the binding energies of either Zr 3d levels or S 2p levels in some other compounds for comparison.

The valence band spectra of $ZrS_{1.29}$ and $ZrS_{.9}$ were measured and compared with the calculated density of states of ZrS with NaCl structure and with WC structure, respectively. The calculations were convoluted with a Gaussian resolution function of 1.0 eV full width half maximum (FWHM). They are shown in Figs. 4.1 and 4.2.

As shown in Table 4.1, the binding energies of the core levels (Zr 3d and S 2p) are insensitive to changing composition in $ZrS_{1.29}$ to $ZrS_{1.34}$.

Comparing the peak positions of the core levels of Zr 3d in $ZrS_{1.29}$ and $ZrS_{.9}$ with those in Zr metal indicates there is some charge transfer in the two structure types of ZrS_{1+x} (superstructure NaCl-type) and of ZrS_{1-x} (WC structure type). Meanwhile, the differences in binding energies of core levels of Zr 3d in $ZrS_{1.29}$ and $ZrS_{.9}$ are systematically different, but this difference is just within

Table 4.1. Binding energies (±.2 eV)

Sample	Phases	$Zr(3d)_{5/2}$	$Zr(3d)_{3/2}$	$S(2p)_{3/2}$	Reference
$ZrS_{1.34}$	ZrS_{1+x}	179.7	182.2	162.1	Present work
$ZrS_{1.29}$	ZrS_{1+x}	179.7	182.2	162.0	Present work
$ZrS^{a}_{\sim 1.0}$	ZrS_{1-x}, small trace of ZrS_{1+x}	179.3	181.8	162.4	Present work
$ZrS_{.9}$	ZrS_{1-x}	179.3	181.8	162.3	Present work
$ZrS^{a}_{\sim .87}$	ZrS_{1-x}, small trace of Zr_2S	179.0	181.5	162.2	Present work
Zr		178.5	181.0		Present work
ZrCl		179.4	181.8		Ref. (41)
MgS				160.8	Ref. (42)
CaS				161.0	Ref. (42)

[a]Compositions were approximated from the starting compositions and material balance. The compositions in other Zr-S samples were analyzed by combustion.

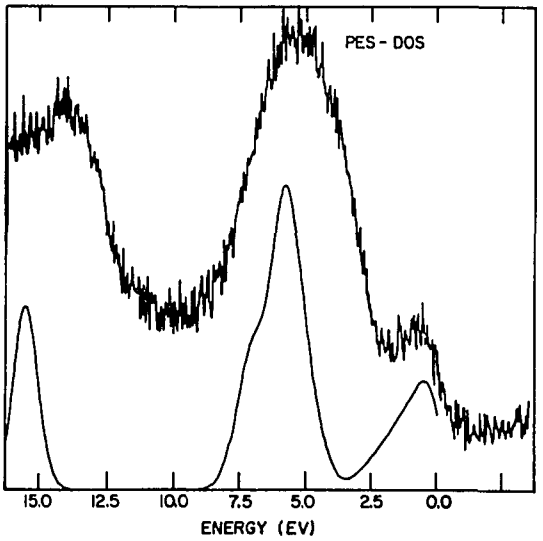

Fig. 4.1. The PES spectrum of the valence band region of $ZrS_{1.29}$ and the DOS of ZrS NaCl-type, convoluted with a Gaussian curve where FWHM is 1.0 eV (smooth curve)

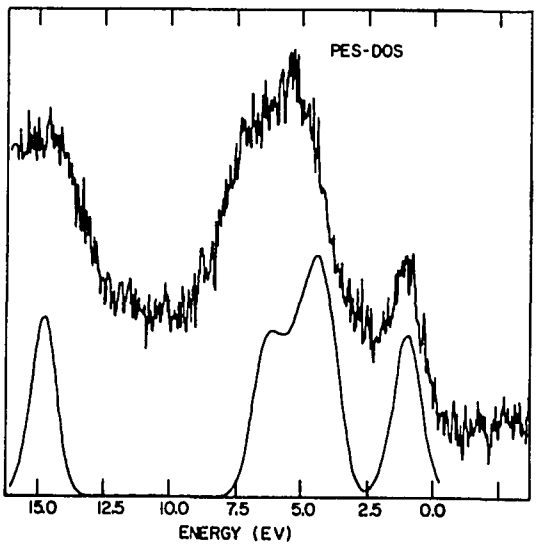

Fig. 4.2. The PES spectrum of the valence band region of $ZrS_{.9}$ and the DOS of ZrS WC-type, convoluted with a Gaussian curve where FWHM is 1.0 eV (smooth curve)

the uncertainty of the instrument. Therefore, it is reasonable to conclude that the charge transfer in ZrS_{1+x} and ZrS_{1-x} are similar, with the ZrS_{1+x} compounds slightly more ionic than the ZrS_{1-x} compounds. The comparison of the sulfur $2p_{3/2}$ in the Zr-S compounds and in CaS or MgS compounds indicates that the charge transfer in ZrS_{1+x} and ZrS_{1-x} is not large enough to cause the sulfur in the Zr-S compounds to have -2 charge, as expected for the sulfur in CaS and MgS compounds.

However, the core levels (Zr $3d_{5/2}$ and Zr $3d_{3/2}$) in $ZrS_{.9}$ are at the same positions as those in ZrCl (41), an unusual layered compound with stacking of Zr and Cl layers, which form stacking units: Cl-Zr-Zr-Cl (43). Therefore, the charge transfer from Zr atoms to S atoms in $ZrS_{.9}$ would be expected to be very similar to the charge transfer from Zr atoms to Cl atoms in ZrCl. Using a self-consistent field band calculation for ZrCl, Marchiando et al. (44) found only .1 electron loss from the zirconium muffin tin sphere.

In Figs. 4.1 and 4.2, the main features are the s band, p band and occupied d band obtained by calculations which seem to have a good correspondence with the valence band spectra of $ZrS_{1.29}$ and $ZrS_{.9}$. Furthermore, a good agreement of the shapes and positions of the d band in the range 2.5 eV $\leq$ B.E. $\leq E_f$ is found between the

calculation and experiment. Also, the split in the calculated density of states of the p band in ZrS (WC-type) was found as the shoulder on the high binding energy side of the p band in the $ZrS_{.9}$ spectrum. However, there are some discrepancies between the calculations and the experiments. The s band was observed at about 14 eV in $ZrS_{1.29}$, while the calculated value for ZrS, NaCl-type is at 15.6 eV. The band widths of the p bands are not well matched with the experimental results. These differences might be caused by the deviations of composition of the studied samples away from the ideal case, 1:1, used in the calculations, and also by the nature of the non-self-consistent field calculation.

V. ELECTRONIC HEAT CAPACITY

A. Background

The heat capacity at low temperature for most normal metallic materials is described by a two term expression

$$C = \gamma T + \beta T^3. \tag{5.1}$$

One term, βT^3, has its origin in the lattice vibration contribution, C_l, according to the Debye model (45). In this model, the lattice contribution to the heat capacity is considered to arise from a distribution of frequencies characteristic of a continuous elastic medium but with an upper limit. There results a lattice heat capacity which has the following form:

$$C_l = (12/5)R\pi^4(T/\theta_D)^3, \tag{5.2}$$

where

R: gas constant,

and

θ_D: Debye characteristic temperature.

The other term, $C_{el} = \gamma T$, originates in the electronic behavior. With the electron gas approximation (45), C_{el} is evaluated by the following equation

$$C_{el} = (1/3)\pi^2 N_A k_B{}^2 N(E_f)T, \tag{5.3}$$

where

k_B = Boltzman constant,

N_A = Avogadro's number,

and

$N(E_f)$ = density of states at the Fermi level for 2 spin directions.

Therefore, γ, the electronic specific heat constant, is given by the expression

$$\gamma = \frac{1}{3} \pi^2 N_A k_B^2 N(E_f). \tag{5.4}$$

By rearranging the equation (5.4), the density of states for both spin directions $N(E_f)$ can be evaluated in terms of the constants and the value of γ, measured from experiments

$$N(E_f) = \frac{3\gamma}{\pi^2 N_A k_B^2} \tag{5.5}$$

Thus with the equation (5.5), the electronic specific heat constant γ of the ZrS_{1-x} and ZrS_{1+x} samples was measured to evaluate their densities of states. The measured densities of states will be compared with the calculated density of states by using the rigid band approximation and the results of the band structure calculations of ZrS (NaCl-type) and ZrS (WC-type).

B. Experiment

About 600 mg - 800 mg of Zr-S samples were pressed into pellets of 1/4" diameter. The γ electronic specific heat constant of the pellets were measured by using the low temperature calorimeter.

The calorimeter was designed to measure small samples in the range of 1 K to 20 K. It operates on a heat pulse principle; a known amount of energy from resistive heating is applied to the sample, and the temperature rise is measured. The heat capacity is determined from the ratio of the energy input to the change in temperature.

A diagram of the calorimeter is shown in Fig. 5.1 and an enlarged picture of the sample chamber is shown in Fig. 5.2. Because extensive descriptions of the calorimeter are found in Refs. (46,47), the calorimeter will only be described briefly in the following sections.

The sample holder was made from .013 cm thick copper foil in the shape of a pan 1.6 cm in diameter and 0.3 cm high along the edge. Six eyelets were silver soldered to the pan to support it in the calorimeter.

The cooler is the helium pot which is a Cu cylinder with a volume about 100 cm^3. Halfway between the top and the bottom of the pot is a plate with an orifice 0.08 cm in diameter. The orifice is necessary to evaporate the liquid helium to cool the helium pot to about 1.2 K.

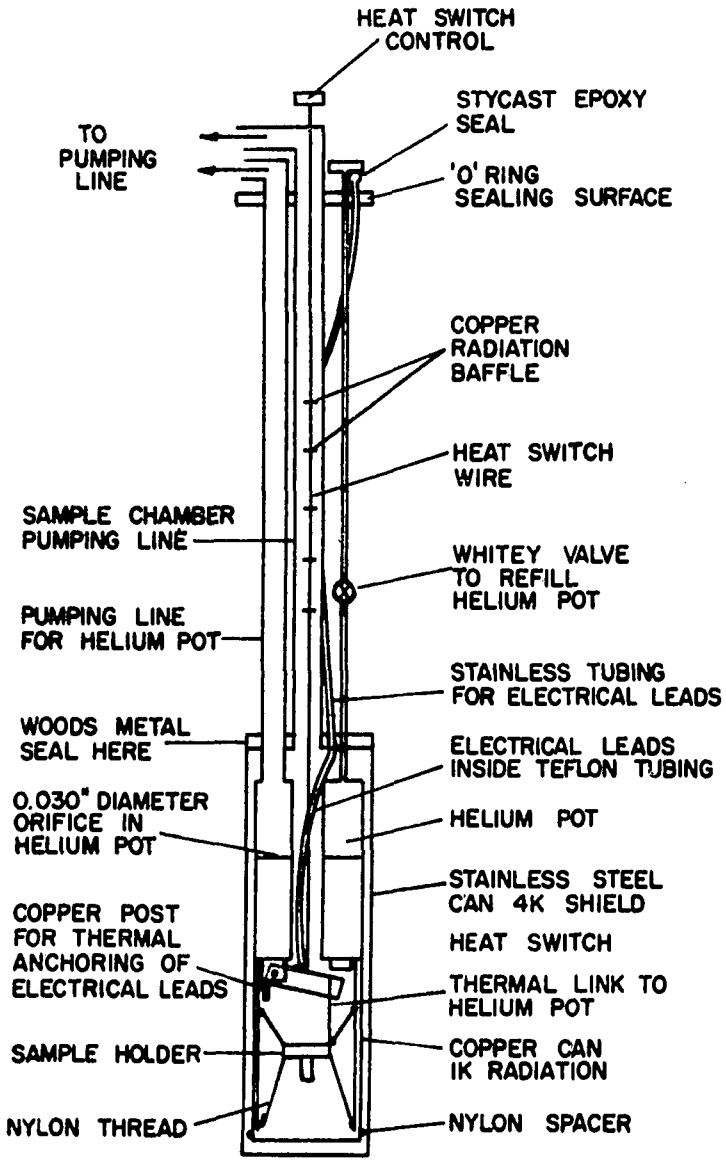

Fig. 5.1. The low temperature calorimeter

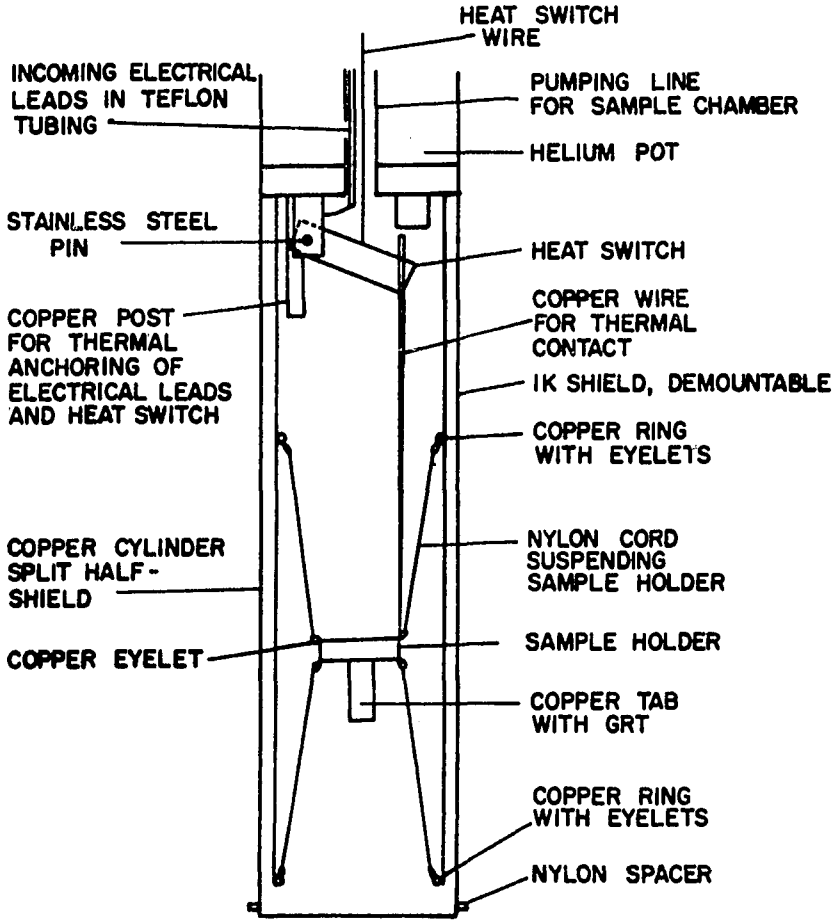

Fig. 5.2. Sample chamber of the calorimeter

The heater was made of a length of 92% Pt and 8% W wire wound noninductively around the side walls of the sample holder pan and secured with G.E 7031 insulating varnish.

The temperature was measured by using a germanium resistance thermometer. The thermometer was attached to the copper foil which was silver soldered to the bottom of the sample holder. The thermometer was also calibrated by C. A. Swenson's research group by a comparison with two standard germanium resistance thermometers. The estimated accuracy is ±0.5 mK from 1 K to 5 K, and ±3.0 mK above 5 K.

To protect the samples from temperature fluctuations, a copper can was mounted directly onto the helium pot to provide a 1 K radiation shield. Outside this shield is a stainless steel can which is maintained at 4.2 K by contact with liquid helium in the helium reservoir. This can was sealed to the system with Wood's metal to provide a good vacuum.

The entire electronic system for the calorimeter is explained in Refs. (46,47).

After the sample pellets and 6 mg of Apiezon N grease (to improve thermal contact of the samples to the sample holder) were mounted on the sample holder, the vacuum can was soldered into place with Wood's metal. The calorimeter was then placed into the Dewar assembly and evacuated to less

than 1 x 10^{-6} torr. (The Dewar assembly is the nitrogen Dewar separated from the interior helium Dewar by a vacuum space.) The nitrogen Dewar was filled and the system cooled by radiation for at least 12 hrs. The liquid helium was then transferred into the helium Dewar and into the helium pot.

Data were taken from about 4.2 K to 10 K, then the samples were cooled to about 1.2 K by pumping on the liquid helium in the helium pot. Data were then collected from 1.2 K to 4.2 K in two consecutive runs. The input heat was determined from the known resistance of the heater, the duration of heat pulse and the known heater current. The duration of heat pulse was measured with a Monsanto digital electronic timer.

The heat capacity of the sample holder with 6 mg Apiezon N (C_{ad}) was determined in advance and was subtracted from the measured heat capacity.

$$C = \frac{\frac{\Delta Q}{\Delta T} - C_{ad}}{X} \tag{5.6}$$

where

ΔQ = the input heat,

ΔT = the incremental temperature rise,

and

X = the number of gram-atoms of the sample.

The heat capacity data were fit to the equation,

$$C/T = \gamma + \beta T^2 \tag{5.7}$$

between 1 K to 5 K by a least squares treatment. The γ values were the intercepts of the plots of C/T versus T^2.

C. Results and Discussion

The measured γ of $ZrS_{1.34}$, $ZrS_{1.30}$, $ZrS_{1.29}$ and $ZrS_{.99}$ are listed in Table 5.1. The graphs of C/T versus T^2 of $ZrS_{1.34}$, $ZrS_{1.3}$ and $ZrS_{.99}$ are shown in Fig. 5.1. The graph of $ZrS_{1.29}$ is very similar to the graph of $ZrS_{1.30}$ due to their closeness in composition. Therefore, the plot C/T versus T^2 of $ZrS_{1.29}$ is not included in Fig. 5.1.

The densities of states were then calculated from the γ values by using equation 5.5. The measured densities of states were also compared with the corresponding calculated densities of states, which were computed either from the results of the band structure calculation of ZrS (NaCl-type) or from the results of the band structure calculation of ZrS (WC-type), by using the rigid band approximation.

The density of states determined by using equation 5.5 has been shown to be enhanced over the actual value by a factor λ (48)

$$N(E_f) = N^{\circ}(E_f)\ (1+\lambda) \tag{5.8}$$

where

$N^{\circ}(E_f)$ = the unenhanced density of states as obtained in a band structure calculation

Table 5.1. Heat capacity in Zr-S samples

Sample	Structure type	No. of valence e[a]	Estimated DOS $\left(\frac{\text{states}}{\text{Ry. molecule}}\right)$	γ (mJ/g-atom K)	Experimental DOS[b] $\left(\frac{\text{states}}{\text{Ry. molecule}}\right)$
$ZrS_{1.34}$[c]	Superstructure of NaCl	8.98	11.82	.70	7.05
$ZrS_{1.30}$[c]	Superstructure of NaCl	9.07	12.38	.99	10.11
$ZrS_{1.29}$[c]	Superstructure of NaCl	9.09	12.56	1.12	11.50
$ZrS_{.99}$[c]	WC	9.96	1.29	.43	4.98

[a]Number of valence electrons were evaluated from the formula units $Zr_{1-x}S$ for the ZrS_{1+x} compounds.

[b]Estimated accuracy for γ's determined from the present work is ±10%, and from reference (7) is ±5%.

[c]Compositions were determined from the combustion analysis.

Table 5.1. (Continued)

Sample	Structure type	No. of valence e[a]	Estimated DOS $\left(\frac{\text{states}}{\text{Ry. molecule}}\right)$	γ (mJ/g-atom K)	Experimental DOS[b] $\left(\frac{\text{states}}{\text{Ry. molecule}}\right)$
$ZrS_{1.17}$[d]	NaCl	9.41	14.46		17.95
$ZrS_{1.20}$[d]	NaCl	9.32	13.82		18.49
$ZrS_{1.29}$[d]	NaCl	9.08	12.44		14.42

[d]From Ref. (7).

and

λ = an enhancement factor due to electron-phonon interactions (λ_{e-p}), electron-electron interactions (λ_{e-e}), and spin fluctuation (λ_{spin}). Generally, the electron-phonon interaction is dominant.

Therefore, without knowledge of λ (usually less than about .5), the calculated density of states $N(E_f)$ is a lower limit of the measured density of states.

As expected, the measured density of states of $ZrS_{.99}$ was higher than the estimated one, as shown in Table 5.1. However, the measured value was much higher than expected if the approximation of λ in equation 5.8 is about .5 is correct. This discrepancy might be explained in terms of the limit of accuracy of nonself-consistent band calculations of the ZrS WC-type, and the limit of accuracy in determining the sample composition. (As shown in Fig. 3.13, a small change in composition of ZrS_{1-x} compound would cause a big jump in the density of states.)

The measured densities of states of $ZrS_{1.34}$, $ZrS_{1.30}$ and $ZrS_{1.29}$ were less than the values estimated from the results of the band structure calculations of ZrS NaCl-type by using the rigid band approximation. However, the measured values showed the same trend as shown by the estimated values, namely with increasing sulfur content

(increasing zirconium vacancies), the density of states decreases. The differences in the measured and estimated density of states indicate that the rigid band approximation is not a valid approximation for the compounds which have compositions which deviate far from the 1:1 ratio.

Nevertheless, the low density of states at the Fermi level could be explained in terms of Peierls transition (49). At compositions which are Zr deficient relative to the ideal case at a ratio 1:1, the Zr vacancies in the Zr-S samples are ordered to give rise to a new structure (superstructure of NaCl-type), and to a new unit cell (6). As a consequence, a new Brillouin zone is formed, yielding a folded set of energy bands, and possibly a different energy band crossing at the fermi level. When such an effect occurs as a result of the energy decrease that accompanies the band splitting and the resultant lowering of portions of energy bands below the Fermi energy, in analogy to a Peierls-type transition, there results a lower density of states at the Fermi level.

Furthermore, these compounds did not show superconducting transitions at 1.3 K or higher temperatures, as shown in the graph in Fig. 5.3. On the other hand, from Moodenbaugh's study on the superconductivity of the Zr-S system, $ZrS_{1.17}$, $ZrS_{1.20}$ and $ZrS_{1.29}$ are found to be superconductors with T_c to be 3.87 K, 3.83 K and less than 1.57 K,

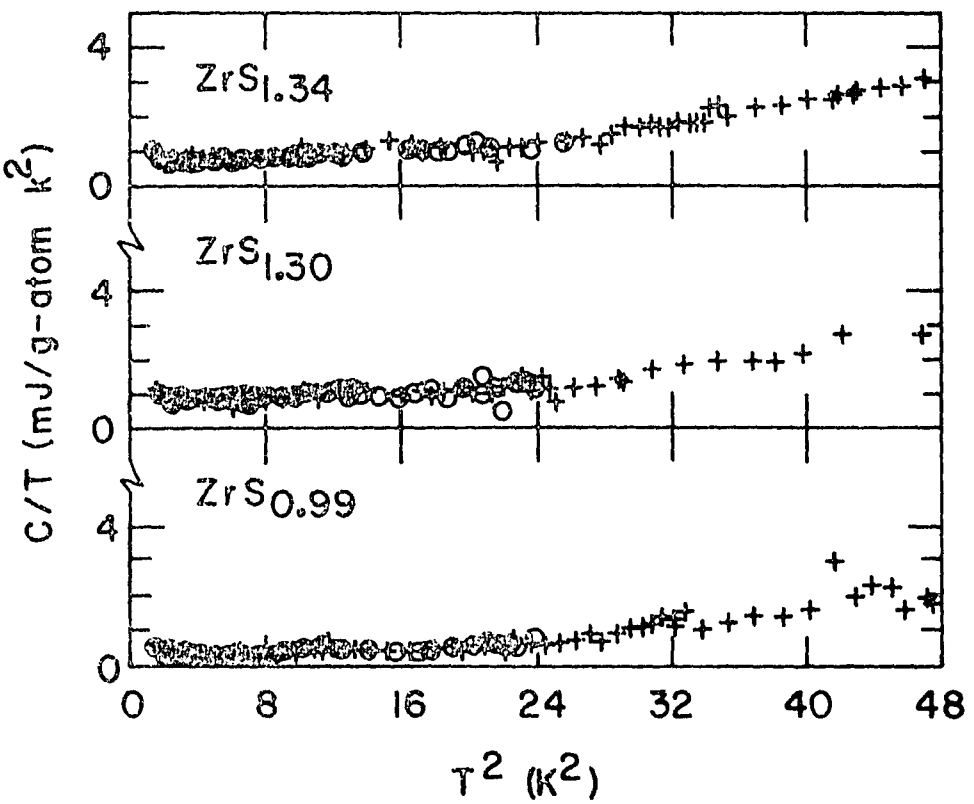

Fig. 5.3. Heat capacity results for the Zr-S samples

respectively (7). However, the superconducting ZrS_{1+x} compounds, which were prepared by the arc-melting method, exist in the NaCl structure with a short-range ordering of vacancies (50), instead of the superstructure of NaCl-type as found in the ZrS_{1+x} compounds studied in the present work. The measured densities of states of the superconducting ZrS_{1+x} are shown to be higher than the estimated values, as well as higher than the measured densities of states evaluated in the present study. The facts are reasonably explained by the nature of superconducting materials, which are prepared by a method which could reasonably be expected to yield metastable samples and which might have higher densities of states at the Fermi level than the thoroughly annealed samples used in the work reported here.

VI. SUMMARY AND CONCLUSION

Two structure types of the thoroughly annealed Zr-S samples, which were found in this work, are the superstructure of the NaCl-type, which correlates with the ZrS_{1+x} compounds, and the WC structure type, which correlates with the ZrS_{1-x} compounds. The homogeneity range of ZrS_{1+x} was determined to be between $ZrS_{1.25\pm.04}$ and $ZrS_{1.35\pm.05}$. Similarly, the homogeneity range of ZrS_{1-x} was from $ZrS_{.89\pm.01}$ to $ZrS_{1.02\pm.03}$. Therefore, by reducing the sulfur content in ZrS_{1+x}, the structure of Zr-S samples is changed from NaCl-type to WC-type. This fact yields questions such as "What are the differences in bonding in NaCl structure and in WC structure?" and "What is the driving force for the structural transition from NaCl-type to WC-type in the Zr-S system?". Using the nonrelativistic LAPW method, the nonself-consistent field band structure of ZrS NaCl-type, and WC-type, which are the simple and perfect samples represented for ZrS_{1+x} and ZrS_{1-x}, respectively, were computed. From the results of calculations, the Zr-S interactions, named as the covalent interactions, were shown to be equally important in both structures. However, the metal-metal interactions are more important in WC structure type than in NaCl structure type. Therefore, it is possible to provide an interpretation of the transition in the

Zr-S system in terms of chemical bonding interactions. The reduction of sulfur content in ZrS_{1+x} results in increasing metal-metal interactions, and this increase favors the WC structure over the NaCl structure.

The photoelectron spectroscopy study on the ZrS_{1+x}, ZrS_{1-x} samples and the Zr metal revealed an observable charge transfer from zirconium atoms to sulfur atoms, as the ionic characteristic displayed by the ZrS_{1+x} and ZrS_{1-x} samples. The charge transfer was observed to be similar in both kinds of sample, and has been approximated to be on the order of 0.1 electron loss from zirconium. This approximation was based on the observation of the equality of chemical shift in binding energies of Zr (3d) core levels in ZrCl and in ZrS_{1-x} samples, and on the value of 0.1 electron loss from Zr muffin tin spheres in ZrCl structure as a result of the self-consistent band structure calculation of ZrCl (43). The valence band spectra of $ZrS_{1.29}$ and $ZrS_{.9}$ showed a remarkable resemblance with the convoluted density of states with 1.0 eV FWHM of ZrS NaCl-type and ZrS WC-type, respectively. This observation indicates the high reliability of the LAPW method used in the electronic structure calculation for ZrS compounds.

The low temperature heat capacity results of $ZrS_{1.34}$, $ZrS_{1.30}$, $ZrS_{1.29}$ and $ZrS_{.99}$ showed no superconducting

transition above 1.3 K for the annealed ZrS_{1+x} and ZrS_{1-x} samples. Again, the calculation is shown to be able to predict the density of states at Fermi level for $ZrS_{1.29}$ (measured: 11.50; calculated: 12.56) higher then the density of states at Fermi level for $ZrS_{.99}$ (measured: 4.98; calculated: 1.29).

VII. REFERENCES

1. a) Franzen, H. F. Prog. Solid St. Chem. 1978, 12, 1; b) Bennett, L. H.; Cuthill, J. R.; McAlister, A. J.; Erickson, N. E.; Watson, R. E. Science 1974, 184, 563.

2. Strotzer, E. F.; Biltz, W.; Meisel, K. Z. anorg. allg. chem. 1939, 242, 249.

3. Hahn, H.; Harder, B.; Mutscke, U.; Ness, P. Z. anorg. allg. chem. 1957, 292, 82.

4. McTaggert, F. K.; Wadsley, A. D. Australian J. Chem. 1958, 11, 445.

5. Conard, B. R.; Franzen, H. F. High Temperature Science 1971, 3, 49.

6. Conard, B. R.; Franzen, H. F. "The crystal structures of ZrS and $Zr_{.77}S$", In Chemistry of Extended Defects in Non-metallic Solids; Eyring, L.; O'Keefe, M., Eds.; North-Holland: Amsterdam, 1970; pp. 207-219.

7. Moodenbaugh, A. R. Ph.D. Dissertation, University of California, San Diego, California, 1975.

8. Conard, B. R. Ph.D. Dissertation, Iowa State University, Ames, Iowa, 1969.

9. Yvon, K.; Jeitschko, W.; Parthé, E. "A Fortran IV Program for the Intensity Calculation of Powder Patterns" (1969 version), School of Metallurgy and Material Science, University of Pennsylvania, Philadelphia, Pennsylvania, 1969.

10. Franzen, H. F.; Smeggil, J.; Conard, B. R. Mat. Res. Bull. 1967, 2, 1807.

11. Graham, J. M.S. Thesis, Iowa State University, Ames, Iowa, 1967.

12. Slater, J. C. J. Chem. Phys. 1964, 41, 3199.

13. Koelling, D. D.; Arbman, G. O. J. Phys. F.: Metal Phys. 1975, 5, 2041.

14. Slater, J. C. Phys. Rev. 1937, 51, 151.

15. Loucks, T. "Augmented Plane Wave Method"; W. A. Benjamin, Inc.: New York, 1967.

16. Herman, F.; Skillman, S. "Atomic Structure Calculations"; Prentice Hall: Englewood Cliffs, New Jersey, 1963.

17. Matheiss, L. F. Phys. Rev. 1963, 133, 184.

18. Löwdin, P. O. Adv. Phys. 1956, 6, 1.

19. Slater, J. C. Phys. Rev. 1951, 81, 385.

20. Harmon, B. N. Ph.D. Dissertation, Northwestern University, Chicago, Illinois, 1973.

21. Pauling, L.; Wilson, E. B. "Introduction to Quantum Mechanics"; McGraw-Hill Book Company, Inc.: New York, 1935.

22. Garbow, B. S.; Dongara, J. J.; Eispack Package, Argonne National Laboratory, Applied Mathematics Division, Technical Memorandum No. 250, 1975.

23. Wilkinson, J. H. "The Algebraic Eigenvalue Problem"; Oxford University Press: London, 1965.

24. Wilkinson, J. H.: Reinsh, C. "Handbook for Automatic Computation", Vol. II "Linear Algebra"; Springer-Verlag: New York, 1971.

25. Gilat, G.; Raubenheimer, L. J. Phys. Rev. 1966, 144, 390.

26. Jepsen, O.; Andersen, O. K. Solid State Commun. 1971, 9, 1763.

27. Walch, P. F.; Ellis, D. E. Phys. Rev. B 1973, 8, 5920.

28. Matheiss, L. F.; Wood, J. H.; Switendick, A. G. Methods in Computational Physics 1968, 8, 64.

29. Schwarz, K.; Pechter, K.; Neckel, A. J. Phys. C: Solid St. Phys. 1975, 8, 1663.

30. Burdick, G. A. Phys. Rev. 1963, 129, 168.

31. Van Dyke, G. A. Sandia Laboratory, Albuquerque, New Mexico, unpublished paper.

32. Stassis, C.; Zarestky, J.; Arch, A.; McMasters, O. D.; Harmon, B. N. Phys. Rev. B 1978, 18, 2632.

33. Neckel, A.; Schwarz, K.; Weinberger, P.; Eibler, R.; Rastle, P. Ber. Bunsenges. Phys. Chem. 1975, 79, 1053.

34. Ramqvist, L.; Manne, R. J. Phys. Chem. Solids 1971, 32, 149.

35. Neckel, A.; Rastl, P.; Eibler, R.; Weinberger, P.; Schwarz, K. J. Phys. C: Solid St. Phys. 1976, 9, 579.

36. Gupta, M.; Gubanov, V. A.; Ellis, D. E. J. Phys. Chem. Solids 1977, 8, 499.

37. Cornwell, J. F. "Group Theory and Electronic Energy Bands in Solids"; North-Holland Publishing Company: New York, 1969.

38. Trogler, W. C.; Ellis, D. E.; Berkowitz, J. J. Am. Chem. Soc. 1979, 101, 5896.

39. England, W. B.; Liu, S. H.; Myron, H. W. J. Chem. Phys. 1974, 60, 3760.

40. Franzen, H. F.; Merrick, J.; Umaña, M.; Khan, A. S.; Peterson, D. T.; McCreary, J. R.; Thorn, R. J. J. Electr. Spectr. and Rel. Phen. 1977, 11, 439.

41. Cisar, A.; Corbett, J. D.; Daake, R. L. Inorg. Chem. 1979, 18, 836.

42. Franzen, H. F.; Umaña, M. X. J. Solid State Chem. 1976, 18, 363.

43. Marchiando, J. F. Ph.D. Dissertation, Iowa State University, Ames, Iowa, 1979.

44. Marchiando, J. F.; Harmon, B. N.; Liu, S. H. "Electronic structure of layered compounds ZrCl, ZrBr, ScCl and PtTe"; International Conference on Layered Compounds: Holland, Aug. 1979.

45. Ziman, J. M. "Principles of the Theory of Solids"; Cambridge University: Cambridge, 1972.

46. Thome, D. V. M.S. Thesis, Iowa State University, Ames, Iowa, 1977.

47. Tsang, T. E. Ph.D. Dissertation, Iowa State University, Ames, Iowa, 1977.

48. McMillan, W. L. Phys. Rev. 1968, 167, 331.

49. Kittel, C. "Introduction to Solid State Physics", 5th ed.; John Wiley & Sons, Inc.: New York, 1976.

50. Kennett, H. M.; Rudee, M. L. Philosophical Magazine 1977, 35, 129.

VIII. ACKNOWLEDGEMENTS

The author would like to take this opportunity to express her sincere gratitude to Professors H. F. Franzen and B. N. Harmon for their guidance, encouragement, patience and many valuable suggestions throughout the entire course of this study.

The author also wishes to thank Dr. Yun Chun for assistance in the low temperature heat capacity study, Mr. J. W. Anderegg for assistance in the photoelectron spectroscopy study and Ms. L. Musselman for her time and effort in typing this dissertation.